Putative pore-forming subunits of the mechano-electrical transduction channel, Tmc1/2b, require Tmie to localize to the site of mechanotransduction in zebrafish sensory hair cells

Itallia V. Pacentine and Teresa Nicolson*

Oregon Hearing Research Center and Vollum Institute, Oregon Health & Science University, Portland, Oregon, United States of America

*Corresponding author

E-mail: nicolson@ohsu.edu

Abstract

Mutations in transmembrane inner ear (*TMIE)* cause deafness in humans; previous studies suggest involvement in the mechano-electrical transduction (MET) complex in sensory hair cells, but TMIE's precise role is unclear. In *tmie* zebrafish mutants, we observed that GFP-tagged Tmc1 and Tmc2b, which are putative subunits of the MET channel, fail to target to the hair bundle. In contrast, overexpression of Tmie strongly enhances the targeting of Tmc2b-GFP to stereocilia. To identify the motifs of Tmie underlying the regulation of the Tmcs, we systematically deleted or replaced peptide segments. We then assessed localization and functional rescue of each mutated/chimeric form of Tmie in *tmie* mutants. We determined that the first putative helix was dispensable and identified a novel critical region of Tmie, the extracellular region and transmembrane domain, which mediates both mechanosensitivity and Tmc2b-GFP expression in bundles. Collectively, our results suggest that Tmie's role in sensory hair cells is to target and stabilize Tmc subunits to the site of MET.

Author summary

Hair cells mediate hearing and balance through the activity of a pore-forming channel in the cell membrane. The transmembrane inner ear (TMIE) protein is an essential component of the protein complex that gates this so-called mechanotransduction channel. While it is known that loss of TMIE results in deafness, the function of TMIE within the complex is unclear. Using zebrafish as a deafness model, Pacentine and Nicolson demonstrate that Tmie is required for the localization of other essential complex members, the transmembrane channel-like (Tmc) proteins, Tmc1/2b. They then evaluate twelve unique versions of Tmie, each containing

38 mutations to different domains of Tmie. This analysis reveals that some mutations in Tmie cause
39 dysfunctional gating of the channel as demonstrated through reduced hair cell activity, and that
40 these same dysfunctional versions also display reduced Tmc expression at the normal site of the
41 channel. These findings link hair cell activity with the levels of Tmc in the bundle, reinforcing
42 the currently-debated notion that the Tmcs are the pore-forming subunits of the
43 mechanotransduction channel. The authors conclude that Tmie, through distinct regions, is
44 involved in both trafficking and stabilizing the Tmcs at the site of mechanotransduction.

45

46 **Introduction**

47 The auditory and vestibular systems detect mechanical stimuli such as sound, gravity, and
48 acceleration. These two systems share a sensory cell type called hair cells. The somas of hair
49 cells are embedded in the epithelium and extend villi-like processes from their apex into the
50 surrounding fluid. The shorter of these, the stereocilia, are arranged in a staircase-like pattern
51 adjacent to a single primary cilium known as a kinocilium. Neighboring cilia are connected by
52 protein linkages. Deflection of the kinocilium along the excitatory axis tugs the interconnected
53 stereocilia, which move as a single unit called the hair bundle [1]. When tension is placed on the
54 upper-most linkages known as tip links, the force is thought to open mechanosensitive channels
55 at the distal end of the shorter stereocilia [2, 3]. These channels pass current, depolarizing the
56 cell and permitting electrical output to the brain via the eighth cranial nerve. The conversion of a
57 mechanical stimulus into an electrical signal is known as mechano-electrical transduction (MET)
58 [4]. The proteins located at the site of MET and involved in gating the MET channel are

59 collectively known as the MET complex. How the components of the MET complex, including
60 the channel itself, are localized to and maintained at the stereocilia tips is not well understood.
61 To characterize the molecular underpinnings of MET and the underlying cause of
62 pathology in human patients, it is essential to examine the individual components of the
63 transduction complex in a comprehensive fashion. Thus far, only a few proteins have been
64 designated as members of the MET complex. The identity of the channel itself remains
65 contentious, but currently the best candidates for the pore-forming subunits are the
66 Transmembrane Channel-like (TMC) proteins TMC1 and TMC2. Mutations in *TMC1* cause
67 human deafness [5], and double knock-outs of mouse *Tmc1/2* result in the loss of MET currents
68 [6-8]. In zebrafish, overexpression of a fragment of Tmc2a generates a dominant negative effect
69 on hair-cell mechanosensitivity [9] and Tmc2a and Tmc2b are required for MET in hair cells of
70 the lateral line organ [10]. The TMCs localize to the tips of stereocilia, the site of MET, in mice
71 and zebrafish [3, 6, 8, 10-12]. A point mutation in mouse *Tmc1* results in altered channel
72 properties, suggesting direct changes to the pore [7, 13]. Likewise, in TMC2 knockout mice,
73 channel permeation properties are altered [14]. Regardless of whether the TMCs are the pore-
74 forming or accessory subunits of the channel, they are essential for MET.
75 Another key component of the complex is Protocadherin-15 (PCDH15), which comprises
76 the lower end of the tip link [15, 16] and interacts with the TMCs [8, 9]. A fourth membrane
77 protein, Lipoma HMGIC fusion partner-like 5 (LHFPL5, formerly called TMHS), interacts with
78 PCDH15 and is critical for localizing PCDH15 to the site of MET [17, 18]. LHFPL5 is also
79 required to properly localize TMC1 in mouse cochlear hair cells [8]. However, loss of LHFPL5
80 in cochlear hair cells does not completely abolish MET currents, and currents can be rescued by
81 overexpression of PCDH15 [18]. This evidence suggests that LHFPL5 is not essential but rather

82 acts as an accessory protein. Another TMC1/2 interacting partner is Calcium and integrin
83 binding protein 2 (CIB2), which is a cytosolic protein that is localized in stereocilia and required
84 for MET in cochlear hair cells [19].

85 A sixth essential member of the MET complex is the transmembrane inner ear (TMIE)
86 protein. Loss of TMIE results in deafness in all vertebrate organisms studied [20-25]. A recent
87 study demonstrated that TMIE is required for active MET channels in cochlear hair cells of mice
88 [26]. These authors showed that despite normal morphology of the inner ear, hair cells lacking
89 TMIE fail to label with aminoglycosides or FM 1-43, both of which are known to permeate the
90 MET channel [27, 28]. TMIE was first localized to the stereocilia of hair cells [29, 30], and then
91 to the stereocilia tips where MET occurs [25]. Zhao et al. further demonstrated that loss of TMIE
92 ablates MET currents, that TMIE interacts with both LHFPL5 and the CD2 isoform of PCDH15,
93 and that interfering with the TMIE-CD2 interaction alters MET. They proposed that TMIE could
94 be a force-coupler between the tip link and channel. However, the CD2 isoform of PCDH15 is
95 only essential in cochlear hair cells and not vestibular hair cells [31]. Zebrafish do not possess
96 the CD2 isoform [9, 32], and yet they still require Tmie for hair-cell function [21]. These
97 findings raised the tantalizing possibility that Tmie might have an additional role in MET that is
98 independent from the tip links. Here, we present an alternative role for Tmie in hair cell function.

99 We first confirmed that mechanosensitivity is absent in a zebrafish mutant of *tmie*,
100 *ru1000*, and demonstrated that this defect is rescued by transgenic Tmie-GFP. The localization
101 of Tmie-GFP is maintained in the absence of other transduction components, suggesting that
102 Tmie traffics independently to hair bundles. Unexpectedly, GFP-tagged Tmcs fail to localize to
103 the hair bundle in *tmie* mutants, and overexpression of Tmie leads to a corresponding increase in
104 bundle expression of Tmc2b-GFP. To determine which regions of Tmie are involved in

105 regulating the Tmcs, we performed a domain analysis of *tmie* by expressing mutated or chimeric
106 transgenes of *tmie* in *tmie*^{ru1000}, and made three key discoveries: (*i*) Tmie can function without
107 its putative first transmembrane domain, (*ii*) the remaining helix (2TM) and adjacent regions are
108 responsible for Tmie's function in hair cells, and (*iii*) dysfunctional *tmie* constructs have reduced
109 efficacy in localizing the Tmcs, supporting the conclusion that impaired MET is due to reduction
110 of Tmc protein. Our evidence suggests that Tmie's role in the MET complex is to promote
111 localization of Tmc1/2 to the site of MET in zebrafish sensory hair cells.

112

113 ## Results

114 **Gross morphology is normal in *tmie*^{ru1000} mutant zebrafish**

115 The literature on TMIE's role in sensory hair cells is somewhat contradictory. Earlier
116 studies proposed a developmental role for TMIE [20-22], while later studies evidenced a role in
117 MET [25, 26]. To begin our analysis and attempt to clarify the issue in zebrafish, we examined
118 live *tmie*^{ru1000} larvae at 5-7 dpf using confocal microscopy. The *ru1000* allele harbors a nonsense
119 mutation leading to an N-terminal truncation, L25X [21]. We observed that mature hair cells of
120 *tmie*^{ru1000} larvae were grossly normal compared to wild type siblings in both the inner ear cristae
121 and the lateral line organ, an organ specific to fish and amphibians (Fig 1A). We noted a slight
122 thinning of the mutant hair bundles, as revealed using a transgene Actin-GFP. Thin bundles have
123 been observed in other zebrafish MET mutants, such as those carrying mutations in *ap1b1* and
124 *tomt.* Both genes have been previously implicated in protein trafficking in hair cells, with *tomt*
125 having a specific role in targeting Tmc1/2 proteins to the hair bundle [11, 33].

126

127 **Tmie-deficient zebrafish are deaf due to a defect in hair cell mechanosensitivity**

128 Next, we used an assay for the auditory evoked behavior response (AEBR) to quantify
129 hearing loss in *tmie*^{ru1000} mutants. We exposed 6 dpf larvae to a loud pure tone stimulus (157 dB,
130 1000 Hz, 100 ms) once every 15 seconds for three minutes and recorded their startle responses
131 (sample traces in Fig 1B). Larvae deficient in *tmie* appear to be profoundly deaf, with little to no
132 response as compared to wild type siblings (Fig 1B and 1C). We then determined basal
133 (unevoked) hair cell activity of *tmie*^{ru1000} larvae using FM 1-43 or FM 4-64. Both are vital dyes
134 that permeate open channels, making them useful as a proxy measure of the presence of active
135 MET channels in hair cells [27, 28, 34]. A 30-second bath application of FM dye readily labels
136 hair cells of the lateral line organ, which are arranged in superficial clusters called neuromasts.
137 We briefly exposed wild type and *tmie*^{ru1000} larvae to FM dye and then imaged the neuromasts
138 (Fig 1D). Consistent with previous findings [21, 22, 26], *tmie*^{ru1000} neuromasts have a severe
139 reduction in FM labeling, suggesting that these hair cells have a MET defect (Fig 1F). To
140 characterize mechanically evoked responses of hair cells, we recorded extracellular potentials, or
141 microphonics (Fig 1H). Using a piezo actuator, we applied a 200 Hz sine wave stimulus to 3 dpf
142 larvae while simultaneously recording voltage responses from hair cells of the inner ear. In
143 agreement with results from our FM dye assay and with microphonic recordings previously
144 reported [21], microphonics are absent in *tmie*^{ru1000} larvae (Fig 1H, gray trace).

145

146 **Transgenic *tmie-GFP* rescues the functional defect in *tmie*^{ru1000} mutants**

147 To rescue mechanosensitivity in *tmie*^{ru1000} larvae, we generated a construct of *tmie* tagged
148 with GFP on its C-terminus, then expressed this transgene using a hair cell-specific promoter,
149 *myosin 6b (myo6b)*. Stably expressed Tmie-GFP rescued the FM labeling in *tmie*^{ru1000} hair cells

150 (Fig 1E and 1F). Tmie-GFP also restores microphonic potentials to wild-type levels (Fig 1H,
151 orange trace). In a stable line with a single transgene insertion, we observed that Tmie-GFP
152 expression varies among hair cells, even within the same patch of neuroepithelium (lateral crista,
153 S1A Fig). Immature hair cells, which can be identified by their shorter stereocilia and kinocilia
154 (S1A Fig, bracket and arrow, respectively), consistently show a bright and diffuse pattern of
155 labeling. This high expression level in immature bundles is characteristic of transgenes expressed
156 using the *myo6b* promoter, which drives expression more strongly in young hair cells [17, 34]. In
157 mature hair cells, expression patterns of Tmie-GFP are variable. At high expression levels, Tmie-
158 GFP is enriched in the bundle in a broader pattern (S1B Fig). At reduced levels, the GFP signal
159 is concentrated at the beveled edge of the hair bundle (S1C Fig). At very low levels, we can
160 observe puncta along the stereocilia staircase, consistent with localization at stereocilia tips (S1D
161 Fig). We suspect that the diffuse "bundle fill" pattern is due to overexpression, and that lower
162 levels of Tmie-GFP recapitulate the endogenous localization at the site of MET, as previously
163 observed in mice [25].
164

165 **Tmie-GFP is capable of trafficking without other members of the MET complex**

166 Having confirmed that our exogenously expressed Tmie-GFP is functional, we used this
167 transgene to probe Tmie's role in the MET complex. First, we characterized Tmie's interactions
168 with other MET proteins *in vivo* by expressing transgenic Tmie-GFP in mutant *pcdh15a*, *lhfpl5a*,
169 and *tomt* larvae (Fig 2). Because a triple knock-out of zebrafish *tmc* has not been reported, we
170 used *tomt* mutants as a proxy for *tmc*-deficient fish based on recent studies of defective bundle
171 localization of the Tmcs in *tomt*-deficient fish and mice [11, 35]. As in wild type bundles (Fig
172 2A), Tmie-GFP is detectable in the stereocilia in each of these MET mutants (Fig 2B and 2D),

173 even if hair bundles are splayed (Fig 2B and 2C, arrowheads). This result suggests that Tmie
174 does not depend on interactions with other MET components for entry into the hair bundle.
175

176 **Tmc1-GFP and Tmc2b-GFP fail to localize to stereocilia without Tmie**

177 To determine if the loss of Tmie affects the other components of the
178 mechanotransduction complex, we expressed GFP-tagged mechanotransduction proteins
179 (Pcdh15aCD3, Lhfpl5a, Tmc1, and Tmc2b) in *tmie*^{ru1000} mutants. Both Pcdh15aCD3-GFP (Fig
180 3A) and GFP-Lhfpl5a (Fig 3B) showed GFP fluorescence in hair bundles with a punctate
181 distribution, similar to the pattern seen in wild type bundles. This result is consistent with the
182 intact morphology of *tmie*^{ru1000} hair bundles. However, when we imaged Tmc1-GFP (Fig 3C) and
183 Tmc2b-GFP (Fig 3E), GFP fluorescence was severely reduced in the hair bundles of *tmie*^{ru1000}
184 mutants. In mature *tmie*^{ru1000} hair cells, we often saw a signal within the apical soma near the
185 cuticular plate, indicative of a trafficking defect (Fig 3E, arrows; position of cuticular plate
186 denoted in Fig 1G). We quantified Tmc expression in the hair bundle region and observed a
187 striking and consistent reduction in *tmie* mutants (Fig 3D and 3F). Previously, we reported that
188 localization of transgenic Tmc-GFP is unaffected in *pcdh15a* mutants [11], demonstrating that
189 mislocalization of Tmc1/2 is not a hallmark of all MET mutants.
190

191 **Overexpression of Tmie increases bundle localization of Tmc2b-GFP**

192 We hypothesized that if the loss of Tmie reduces Tmc localization in the hair bundle,
193 then overexpression of Tmie may have the opposite effect. To test the consequence of
194 overexpression of Tmie on Tmc localization, we created a second construct of *tmie* coupled with
195 *p2A-NLS(mCherry)* driven by the *myo6b* promoter. The p2A linker is a self-cleaving peptide,

196 which leads to translation of equimolar amounts of Tmie and NLS(mCherry). Hence, mCherry
197 expression in the nucleus denotes Tmie expression in the cell (Fig 3G, lower panels). We
198 generated a stable *tmie*^{ru1000} fish line carrying the *tmie-p2A-NLS(mCherry)* transgene and then
199 crossed it to the *Tg(myo6b:tmc2b-GFP); tmie*^{ru1000} line. We observed that overexpression of
200 Tmie led to a 2.5-fold increase in expression of Tmc2b-GFP in the bundles of hair cells when
201 compared to wild type siblings that carried only the *tmc2b-GFP* transgene (Fig 3G and 3H).
202 Combined with the finding that Tmc expression is lost in hair bundles lacking Tmie, our data
203 suggest that Tmie positively regulates Tmc localization to the hair bundle.
204

205 **Transgenes can effectively determine protein functionality**

206 To gain a better understanding of Tmie's role in regulating the Tmcs, we characterized a
207 new allele of *tmie*, *t26171*, which was isolated in a forward genetics screen for balance and
208 hearing defects in zebrafish larvae. Sequencing revealed that *tmie*^{t26171} fish carry an A→G
209 mutation in the splice acceptor of the final exon of *tmie*, which leads to use of a nearby cryptic
210 splice acceptor (S2A Fig, *DNA, cDNA*). Use of the cryptic acceptor causes a frameshift that
211 terminates the protein at amino acid 139 (A140X), thus removing a significant portion of the C-
212 terminal tail (S2A Fig, *Protein*). Homozygous mutant larvae exhibit severe auditory and
213 vestibular deficits, being insensitive to acoustic stimuli and unable to maintain balance (S2A Fig,
214 *Balance*). FM 4-64 labeling of *tmie*^{t26171} mutant hair cells suggests that the effect of the mutation
215 is similar to the *ru1000* mutation (S2B and S2D Figs). This finding implicates the C-terminal
216 tail, a previously uncharacterized region, in Tmie's role in MET. However, when we
217 overexpressed a near-mimic of the predicted protein product of *tmie*^{t26171} (1-138-GFP) using the
218 *myo6b* promoter, we observed full rescue of FM labeling defects in *tmie*^{ru1000} (S2C and S2D

219 Figs), as well as behavioral rescue of balance and acoustic sensitivity (n=19). These results
220 revealed that when expressed at higher levels, loss of residues 139-231 does not have a
221 significant impact on Tmie's ability to function.

222 This paradoxical finding highlighted an important advantage of the use of transgenes over
223 traditional mutants. There are myriad reasons why a genomic mutation may lead to dysfunction,
224 including reduced transcription or translation, protein misfolding and degradation, or
225 mistrafficking. Exogenous expression may overcome these deficiencies by producing proteins at
226 higher levels. Moreover, the use of transgenes enabled us to carry out a more comprehensive
227 structure/function study of Tmie. To test a collection of deletions and chimeras of Tmie, we
228 therefore used the *myo6b* promoter to drive exogenous expression of the constructs in hair cells
229 of the *tmie*^{ru1000} mutant.

230 We systematically deleted or replaced regions of *tmie* to generate 12 unique *tmie*
231 constructs (Fig 4A). Earlier studies in zebrafish and mice proposed that Tmie undergoes
232 cleavage, resulting in a single-pass mature protein [21, 36]. To test this hypothesis, we generated
233 the SP44-231 construct of Tmie, which replaced the N-terminus with a known signal peptide
234 (SP) from a zebrafish Glutamate receptor protein (Gria2a). The purpose of the unrelated signal
235 peptide was to preserve the predicted membrane topology of Tmie. We also made a similar
236 construct that begins at amino acid 63, where the sequence of Tmie becomes highly conserved
237 (*SP63-231*). Three of the constructs contained internal deletions (*Δ63-73; Δ97-113; Δ114-138).*
238 In three more constructs, we replaced part of or the entire second transmembrane helix (2TM)
239 with a dissimilar helix from the CD8 glycoprotein (*CD8; CD8-2TM; 2TM-CD8*). We included
240 our mimic of the zebrafish *tmie*^{t26171} mutant, which truncates the cytoplasmic C-terminus (*1-*
241 *138*). To further truncate the C-terminus, we made a construct that mimics the mouse *sr*^{J} mutant

242 (*1-113*). In mice, this truncation recapitulates the full-deletion phenotype [20]. Finally, we
243 included an alternate isoform of Tmie that uses a different final exon, changing the C-terminal
244 sequence (*Tmie-short*). This isoform is found only in zebrafish [21] and its function has not been
245 explored.
246

247 **Subcellular localization of mutated or chimeric Tmie reveals domains required for self-**
248 **localization to the bundle**

249 We first determined the subcellular localization of each Tmie fusion protein. Plasmid
250 DNA was co-injected into *tmie*^{ru1000} eggs with transposase to generate mosaic expression of the
251 constructs in a subset of hair cells. At 4-6 days post injection, we imaged individual hair cells
252 expressing each transgene (Fig 4B). To quantify the enrichment in the bundle versus soma, we
253 measured the integrated density of GFP fluorescence in a small central area of mature bundles
254 (Fig 4C, black oval) and separately in the plasma membrane or soma-enriched compartments
255 (Fig 4C, magenta oval). Correcting for area, we then divided the bundle values by the total
256 values (bundle/bundle + soma) and expressed this as a ratio (Fig 4D). Values closer to 1 are
257 bundle enriched, while values closer to 0 are soma-enriched. We excluded the *CD8-GFP*
258 construct from further analyses because it was detected only in immature bundles (Fig 4B, *CD8*).

259 Localization fell into three broad categories: bundle-enriched, soma-enriched, and
260 equally distributed. Most of the fusion proteins were bundle-enriched, similar to full-length
261 Tmie-GFP expression (Fig 4B and 4D). Three constructs were trafficked to the bundle but also
262 expressed in the soma (*SP63-231, CD8-2TM, 1-138*). This result suggests that the deleted
263 regions in these constructs have some role in designating Tmie as a bundle-localized protein.
264 Also of note, the full replacement of the 2TM helix (*CD8*) was unable to maintain stable

265 expression in mature bundles. Half-TM replacements (*CD8-2TM, 2TM-CD8*) revealed that loss
266 of the first half of the helix affects trafficking, whereas alteration of the second half had no
267 effect. Only two constructs were soma-enriched (*Tmie-short* and *1-113*), suggesting an inability
268 to traffic to the bundle. These two transgenes were thus excluded from further analyses.
269

270 **FM labeling identifies functional regions in the second transmembrane domain and**
271 **adjacent residues of Tmie**

272 To identify regions of Tmie involved in mechanosensitivity of hair cells, we measured
273 the functionality of the nine *tmie* constructs that showed hair bundle expression. As in Fig 1F, we
274 generated stable lines of each transgenic construct and quantified fluorescence in neuromasts
275 after exposure to FM 4-64 (Fig 5).

276 Of nine constructs examined, four showed wild type levels of FM fluorescence in
277 *tmie*^{ru1000} neuromasts (*Tmie, SP44-231, Δ114-138*, and *1-138;* Fig 5A and 5B). Two constructs
278 (*Δ97-113* and *Δ63-73*) did not rescue above mutant levels of FM 4-64, although Δ63-73 showed
279 a non-significant increase in FM fluorescence. While residues 63-73 have not been characterized,
280 the Δ97-113 result is consistent with the findings of previous publications in humans and mice,
281 showing that mutations in this region impair hearing and hair cell function [23, 25]. Three
282 constructs were capable of partial rescue (*SP63-231, CD8-2TM,* and *2TM-CD8*). Each one of the
283 five dysfunctional constructs altered part of a contiguous region of Tmie: the 2TM and
284 surrounding domains. These results highlight this region of Tmie as vital for function. To
285 determine whether any of the constructs also have a dominant effect on hair-cell function, we
286 compared FM label in wild type larvae with or without the individual transgenic *tmie* construct
287 (Fig 5D). SP63-231 and Δ63-73, which had impaired rescue in *tmie*^{ru1000}, showed reduced FM

288 label in transgenic wild type cells (Fig 5C and 5D). Interestingly, these two dominant negative
289 constructs alter the extracellular region of Tmie.
290

291 **Recordings of mechanically evoked responses confirm that the second transmembrane**
292 **domain and adjacent regions are required for hair cell function**

293 Bath applied FM dye demonstrates the presence of permeable MET channels, but does
294 not reveal any changes in mechanically evoked responses in hair cells. Therefore, we also
295 recorded microphonics of mutant larvae expressing individual transgenes. For our recordings, we
296 inserted a recording pipette into the inner ear cavity of 3 dpf larvae and pressed a glass probe
297 against the head (Fig 6A). Using a piezo actuator to drive the probe, we delivered a step stimulus
298 at increasing driver voltages while recording traces in current clamp (Fig 6B). For each
299 transgenic *tmie* line, we measured the amplitude of the response at the onset of stimulus (Fig 6C-
300 I). We limited our analysis to the lines expressing constructs that failed to fully rescue FM
301 labeling (Fig 6E-I). As positive controls, we used the full-length *tmie* line (Fig 65 C) and also
302 included *SP44-231* (Fig 6D), encoding the cleavage product mimic. Both controls fully rescued
303 the responses in *tmie*^{ru1000} larvae. Consistent with a reduction in labeling with FM dye, we found
304 that the microphonic responses were strongly or severely reduced in larvae expressing the *SP63-*
305 *231, Δ63-73, CD8-2TM*, *2TM-CD8* and *Δ97-113* constructs in the *tmie*^{ru1000} background (Fig 6E-
306 I). We also saw the same dominant negative effect in wild type larvae expressing transgenic
307 *SP63-231* or *Δ63-73*.
308

309 **Regions of Tmie that mediate hair-cell mechanosensitivity are also required for localizing**
310 **Tmc2b-GFP**

311 After identifying functional regions of Tmie, we asked whether these regions are
312 involved in regulating Tmc localization. Therefore we quantified hair bundle expression of
313 transgenic Tmc2b-GFP in hair cells of *tmie*^{ru1000} mutant larvae stably co-expressing individual
314 transgenic *tmie* constructs (Fig 7B-H). As in Fig 3 G, we tagged our *tmie* constructs with p2A-
315 NLS(mCherry) so that Tmc2b-GFP expression in the hair bundles could be imaged separately.
316 We examined SP44-231 and the five *tmie* constructs that yielded impaired mechanosensitivity.

317 Three constructs showed full rescue of Tmc2b-GFP levels in the bundle. The SP44-231
318 cleavage mimic produced highly variable levels, some in the wild type range, others increasing
319 Tmc2b-GFP expression above wild type (Figs 7B and 7H), as seen in overexpression of full-
320 length Tmie (Figs 3H and 7A, right panel). We suspect that the exogenous Gria2a signal peptide
321 leads to variable processing of Tmie and thus contributes to this variability in Tmc2b-GFP
322 fluorescence. *tmie*^{ru1000} larvae expressing the SP63-231 construct gave rise to values of Tmc2b-
323 GFP fluorescence within the wild type range (Fig 7C and 7H). When we recorded microphonics
324 in these larvae, we found that co-overexpression of Tmc2b-GFP and SP63-231 resulted in better
325 functional rescue of *tmie*^{ru1000} (S3A Fig) than when SP63-231 was expressed alone (Fig 6E). We
326 also determined that the microphonic potentials correlated with the levels of Tmc2b-GFP in the
327 bundles (S3B Fig). Likewise, the 2TM-CD8 construct also generated values of Tmc2b-GFP
328 fluorescence in the wild type range (Fig 7F and 7H). These larvae rescued microphonic
329 potentials to wild type levels (S3C Fig), unlike when 2TM-CD8 was expressed alone (Fig 6E).
330 Functional rescue again correlated with Tmc2b-GFP bundle levels (S3D Fig). These results
331 indicate that functional rescue in the SP63-231 and 2TM-CD8 lines is Tmc dose-dependent.

332 Of the three constructs with little to no functional rescue, CD8-2TM (Fig 7E and 7H) and
333 Δ97-113 (Fig 7G and 7H) had severely reduced levels of Tmc2b-GFP in hair bundles. In
334 *tmie*^{ru1000} expressing Δ63-73, there was severely reduced but still faintly detectable Tmc2b-GFP
335 signal though, as with the functional rescue, this difference was not statistically significant (Fig
336 7D and 7H). The bulk of this signal was observed in immature bundles (Fig 7D, arrows, and S4
337 Fig), but there was some detectable Tmc2b-GFP signal in mature bundles (S4 Fig). Overall,
338 these results suggest that the level of functional rescue by the *tmie* constructs is correlated to the
339 amount of Tmc2b present in the hair bundle.
340

341 **Discussion**

342 *TMIE* was first identified as a deafness gene in mice and humans [20, 23]. The predicted
343 gene product is a relatively small membrane protein containing a highly conserved amino acid
344 sequence near the second hydrophobic helix. Previous studies established that TMIE is required
345 for MET in hair cells [21, 25, 26] and is an integral member of the complex (Zhao et al., 2014).
346 How TMIE contributes to the function of the MET complex was not clear. Our comprehensive
347 structure-function analysis of Tmie revealed that the functional capacity of various *tmie* mutant
348 constructs is determined by their efficacy in localizing Tmc2b-GFP to the bundle, as summarized
349 in Fig 8A and modeled in Fig 8B. These findings unveil a hitherto unexpected role for Tmie in
350 promoting the localization of the putative channel subunits Tmc1 and Tmc2b to the site of MET.
351 These findings broaden our understanding of the assembly of the MET complex and point to a
352 pivotal role of Tmie in this process.
353 A previous study of the *ru1000* mutant suggested that Tmie's role in zebrafish hair cells
354 was developmental, with mutant lateral line hair cells showing stunted kinocilia and the absence

355 of tip links [21]. In our hands we did not observe any gross morphological defects, and the
356 localization pattern and the levels of Pcdh15a and Lhfpl5a were unaffected in *tmie*^{ru1000} larvae.
357 This observation is consistent with intact hair bundle morphology; stereocilia that are splayed or
358 disorganized are a dominant feature of hair cells missing their tip links, as seen in *pcdh15a* or
359 *lhfpl5a* mutants [17, 32]. In TMIE-deficient mice, hair cell morphology is grossly normal up to
360 P7 [25, 26]. In agreement with a previous study in mice [25], our results indicate that *tmie*^{ru1000}
361 mutants are profoundly deaf due to ablation of MET in hair cells. We fully rescued this deficit in
362 zebrafish *ru1000* mutants by exogenous expression of a GFP-tagged transgene of *tmie*.
363 Exogenous expression gave rise to variable levels of Tmie-GFP in hair bundles, with lower
364 levels revealing a punctate pattern expected for a member of the MET complex, and higher
365 expression levels leading to expression throughout the stereocilia. Excess Tmie-GFP did not
366 appear to cause adverse effects in hair cells, which is consistent with a previous study in the
367 *circler* mouse mutant [37].
368

369 **Tmie can localize to hair bundles independently**

370 To determine the interdependence of trafficking of Tmie and the other MET components,
371 we examined the localization of Tmie-GFP in mutants of essential MET genes: the tip-link
372 protein *pcdh15a*; the accessory protein *lhfpl5a*; and in *tomt* mutants (Fig 3). In both zebrafish and
373 mice, the secretory pathway protein Tomt is required for proper localization of the Tmc1/2 [11,
374 35]; the *tomt* mutant likely simulates the condition of a triple knockout of all three zebrafish *tmc*
375 genes (*tmc1/2a/2b*). Despite the absence of Pcdh15a, Lhfpl5a, and Tmcs, we found that Tmie-
376 GFP still traffics to the bundles of hair cells. This finding suggests that Tmie can localize
377 independently of the other proteins of the MET apparatus. This autonomy is an unusual feature

378 for membrane components of the MET complex. For example, PCDH15 largely requires
379 LHFPL5 for trafficking to the stereocilia [17, 18, 38], and depends on Cadherin 23 to maintain
380 its localization at the site of MET [17, 39]. LHFPL5 also requires PCDH15 to maintain
381 localization at the stereocilia tips [18, 38]. Thus, Tmie appears to be the exception to the rule of
382 co-dependent transport to the hair bundle.

383 Our results reveal that Tmie has distinct regions associated with self-localization and
384 function (Fig 8). Three constructs showed impaired targeting of Tmie to the bundle, namely
385 SP63-231, CD8-2TM, and the 1-138 construct, the last of which truncates the C-terminus.
386 Further manipulation to the C-terminus, either by removing more amino acids (*1-113*) or by
387 using an alternative final exon (*Tmie-short*), results in targeting of the protein to the plasma
388 membrane instead of the bundle. However, removing just a smaller internal segment has no
389 effect on bundle localization (Fig 4A and 4C, *Δ114-138*). We suspect that the abundance of
390 charged residues in the C-terminus of Tmie (S2A Fig, *Protein*), as well as the regions altered in
391 SP63-231 and CD8-2TM, contribute to recognition by bundle trafficking machinery.
392 Mislocalization, however, did not necessarily correlate with functional rescue. Despite partial
393 mislocalization to the plasma membrane, the 1-138 construct showed full functional rescue.
394 Conversely, despite normal localization to the bundle, Δ97-113 did not rescue function at all.
395 These results demonstrate that Tmie's functional role is separate from its ability to target to the
396 bundle.
397

398 **Tmie promotes the levels of Tmc1/2 in the hair bundle**

399 The regulatory role of Tmie with respect to the Tmcs is strongly supported by the
400 strikingly different effects of loss of Tmie versus overexpression of Tmie. When Tmie is absent,

401 so are the Tmcs; when Tmie is overexpressed, the level of Tmc2b in the bundle is boosted as
402 well (Fig 3C-H). These results disagree with a previous finding in mice showing that Myc-
403 TMC2 is present in hair bundles of TMIE-deficient cochlear hair cells [25]. This discrepancy
404 may be due to the use a cytomegalovirus promoter to drive high levels of expression of Myc-
405 TMC2 in an *in vitro* explant of cochlear tissue. Localization of TMC1 in *Tmie-/-* mice, which is
406 the predominant TMC protein in cochlear hair cells, was not reported. In addition, localization of
407 the TMCs in vestibular hair cells was not characterized in *Tmie-/-* mice. Thus, further
408 investigation is warranted to determine if the relationship between Tmie and the Tmcs uncovered
409 by our experiments is a conserved feature or is potentially dependent on the type of hair cell, as
410 MET components may vary among different cell types.
411 One important question is whether Tmie and the Tmcs can physically interact to form a
412 complex that is transported to the hair bundle. A direct interaction of the mouse TMC1/2 and
413 TMIE proteins was not detected in a heterologous system [25], however, our *in vivo* analysis
414 suggests the possibility of an indirect interaction. The deletions and chimeric forms of Tmie in
415 the present study highlight important motifs or regions of Tmie that are critical for localization of
416 the Tmcs to the hair bundle.
417
418 **The first hydrophobic helix of Tmie is dispensable**
419 The membrane topology of Tmie has not been biochemically determined, however,
420 online *Phobius* software predicts an N-terminal signal peptide in mouse and human TMIE and a
421 transmembrane helix in zebrafish Tmie [40]. Interestingly, the orthologues in C. elegans or
422 Drosophila do not contain this first hydrophobic region of Tmie. Upon removal of this region,
423 we observed that SP44-231 behaved like full-length Tmie, with a comparable pattern of

424 localization and full functional rescue of *tmie*-deficient fish. In addition, SP44-231 rescues
425 Tmc2b-GFP bundle expression to wild type levels or higher. To our knowledge, these results are
426 the first *in vivo* evidence that Tmie can function without the putative first transmembrane
427 domain. Our study supports the notion that Tmie undergoes cleavage, resulting in a single-pass
428 membrane protein that functions in the MET complex (Fig 8B).
429

430 **The 2TM domain and adjacent regions of Tmie are functionally significant**

431 The key functional domains of Tmie are located within and proximal to the remaining
432 transmembrane domain. We found that replacement of the entire transmembrane domain with an
433 exogenous membrane helix from the CD8 glycoprotein resulted in a protein that trafficked to the
434 bundles of immature hair cells but was not expressed in mature bundles. This finding
435 demonstrates that this domain is vital for stable localization of Tmie in mature hair cells. Half-
436 chimeras of this domain revealed that the mislocalization effect is exclusive to the first half of
437 the helix, but that both halves are functionally significant (the first half more so than the second).
438 These results suggest that the transmembrane domain is critical for both Tmie's localization and
439 function in the MET complex.

440 Removal of the cytoplasmic amino acids 97-113, directly after the 2TM, leads to a
441 normal localization pattern but complete loss of function. This region contains arginine residues
442 that have previously been implicated in human deafness [23, 41-43]. Mimics of these mutations
443 in mouse cochlear hair cells lead to altered MET currents, which has been attributed to a
444 reduction in binding to PCDH15-CD2 [25]. Interestingly, one of the mouse mutations, R93W,
445 resulted in loss of TMIE localization at the site of MET. In contrast to these findings, when we
446 remove this entire intracellular region from zebrafish Tmie, it is still capable of localization in

447 hair bundles. This result may reflect species differences in recognition sequences for trafficking
448 machinery.
449 The SP63-231 and Δ63-73 constructs both lack different segments of the extracellular
450 region of Tmie. These were the only two constructs with dominant negative effects, suggesting
451 that each construct successfully integrates into the MET complex and interferes or competes with
452 endogenous Tmie. Both constructs only minimally rescue mechanosensitivity in *tmie*^{ru1000}
453 mutants and are thus predicted to weaken the efficiency of the MET complex. Other constructs
454 such as the transmembrane chimeras also yield partial rescue but do not appear to affect the
455 function of endogenous Tmie in wild-type hair cells. These data suggest that the full 2TM
456 domain is required to produce the dominant negative effect on endogenous Tmie. Combined with
457 the finding that replacement of the 2TM with an unrelated helix causes instability of Tmie in
458 mature hair cells, we suggest that the 2TM is essential in integrating Tmie into the MET
459 complex.
460
461 **Impaired functionality corresponds to decreased Tmc expression**
462 When co-expressed with Tmc2b-GFP, our Tmie constructs reveal a strong link between
463 function and Tmc bundle expression (Figs 7 and S3). In larvae expressing CD8-2TM and Δ97-
464 113, both of which display little or no functional rescue, there is no detectable Tmc2b-GFP in the
465 hair bundle (Fig 7E, 7G and 7H). In addition to defects in targeting Tmcs to the hair bundle, our
466 data also suggest a role for Tmie in maintaining the levels of Tmc2b in stereocilia. The most
467 dramatic effect on maintenance of Tmc signal in the bundle was seen in *tmie*^{ru1000} larvae
468 expressing the Δ63-73 construct. In these larvae, Tmc2b-GFP successfully traffics to the bundle
469 in immature hair cells (Fig 7D, arrows) but does not maintain strong expression in mature cells

470 (S4 Fig). Based on this data, we conclude that the first half of the transmembrane domain and the
471 intracellular residues 97-113 are involved in trafficking the Tmcs to the site of MET, while the
472 extracellular residues 63-73 stabilize Tmc expression in the MET complex (Fig 8B).

473 Surprisingly, SP63-231 and 2TM-CD8 rescue Tmc2b-GFP to wild type levels (Fig 7C,
474 7F and 7H), even though functional rescue of *tmie*^{ru1000} by GFP-tagged versions was reduced in
475 both FM labeling experiments (Fig 5) and microphonic recordings of the inner ear (Fig 6). This
476 result hints at an additional role for Tmie in MET that is independent of Tmc trafficking.
477 However, the low level of functional rescue in *tmie*^{ru1000} mutants by these two constructs was
478 only observed in the background of endogenous levels of the Tmcs. When we co-expressed
479 Tmc2b-GFP with either SP63-231 or 2TM-CD8, then the functional rescue of *tmie*^{ru1000}
480 mechanosensitivity improved in a Tmc-dose-dependent manner (S3 Fig). Since co-expression of
481 Tmc2b-GFP can overcome the functional deficit in SP63-231 and 2TM-CD8, we propose that
482 residues 44-62 and the second half of the 2TM are important but not absolutely essential to
483 regulating Tmc bundle expression. This finding reinforces the significance of our findings with
484 the constructs Δ63-73, CD8-2TM, and Δ97-113, which still fail to rescue Tmc2b-GFP levels
485 even when Tmc2b-GFP is co-expressed.

486 Through a systematic *in vivo* analysis of *tmie* via transgenic expression, we identified
487 new functional domains of Tmie. We demonstrated a strong link between Tmie's function and
488 Tmc1/2 expression in the bundle. Evidence continues to mount that the Tmcs are subunits of the
489 MET channel, and our results implicate Tmie in promoting and maintaining the localization of
490 Tmc subunits at the site of MET. The precise mechanism underlying Tmie's regulation of the
491 Tmcs awaits further investigation.

492

493 # Methods

494

495 **Zebrafish husbandry**

496 Zebrafish (*Danio rerio*, txid7955) were maintained at 28°C and bred according to
497 standard conditions. All animal research was in compliance with guidelines from the Institutional
498 Animal Care and Use Committee at Oregon Health and Science University. In this study, the
499 following zebrafish mutant lines were used: *tmie*^{ru1000} [21], *tmie*^{t26171}, *pcdh15a*^{psi7} [9],
500 *lhfpl5a*^{tm290d} [44], *tmc2b*^{sa8817} [11]. All zebrafish lines in this study were maintained in a
501 Tübingen or Top long fin wild type background. We examined larvae at 4-7 days post-
502 fertilization (dpf), of undifferentiated sex. For experiments involving single transgenes, non-
503 transgenic *tmie*^{ru1000} heterozygotes were crossed to transgenic fish in the homozygous or
504 heterozygous *tmie*^{ru1000} background. Mutants were genotyped by PCR and subsequent digestion
505 or DNA sequencing. Primers are listed in Table 1.

506

507 **Table 1. List of primers used in this study.**

Primers for plasmid construction		
Plasmid	Forward (5' - 3')	Reverse (5' - 3')
pME-Tmie	GGGGACAAGTTTGTACAAAAAAGCAGGCTCCAAAC ATGAGACGCGGGAGAAGAA	GGGGACCACTTTGTACAAGAAAGCTGGGTC TTTCTTCGCAGGCTTCTTGG
pME-SP44-231	GGGGACAAGTTTGTACAAAAAAGCAGGCTCCAAAC ATGATTTTGTCGGGTCTCCTTTTACCCGCGTTATGG GGACTGGCGCTCGGCCAGATACCAGACCCAGAGCT	same as pME-Tmie
pME-SP63-231	ACCTCAGAAACAGTGGTGTTTTGGGGA	GCCGAGCGCCAGTCCC
pME-Δ63-73	TTATGGCAGGTTGTGGGCATTTTC	GACGGGGTCTGGCTTTTTCG

pME-CD8	PCR 1	same as pME-Tmie	GAGAAGGACCCCACAAGTCCCGGCCAGGGGCGCCCAGATGTATCGAAGTCCCCAAAACAC
	PCR 2	TTGTGGGGTCCTTCTCCTGTCACTGGTTATCACCCTTTACTGCAAATGCCGAATCCCAC	same as pME-Tmie
pME-CD8-2TM	PCR 1	ATGAGACGCGGGAGAAGAAGAGGGAAAATG	CCCACAAGTCCCGGCCAGGGGCGCCCAGATGTATCGAAGTCCCCAAAACACCACTGTTTC
	PCR 2	TGGCCGGGACTTGTGGGATCTTAGCAATAATAATTACGCTCTGCTGCATCTTCAAATGCC	TTTCTTCGCAGGCTTCTTGGCACCTC
pME-2TM-CD8	PCR 1	same as pME-CD8-2TM	AAAGGGTGATAACCAGTGACAGGAGAAGGACGAACATGGAGAAAATGCCCACAACCTGCC
	PCR 2	CCTTCTCCTGTCACTGGTTATCACCCTTTACTGCAAATGCCGAATCCCACGGACG	same as pME-CD8-2TM
pME-Δ97-113		AGACTTGCTGCGAAAAATTATGCCAAC	GAAGATGCAGCAGAGCGTAATTATTATTGC
pME-Δ114-138		GCGGCAAAGGTTGAGGTGAAG	TTGCGCGTGCCGAGC
pME-1-138		same as pME-Tmie	GGGGACCACTTTGTACAAGAAAGCTGGGTCGCCGGGCACCTCAG
pME-1-113		same as pME-Tmie	GGGGACCACTTTGTACAAGAAAGCTGGGTCTTGCGCGTGCCGAG
pME-Tmie-short		same as pME-Tmie	GGGGACCACTTTGTACAAGAAAGCTGGGTCAGTGCCAGGATTGGCTG

508

509 **Gene accession numbers for mutants and transgenes**

510 *tmie* (accession no. F1QA80), *tmc1* (accession no. F1QFU0), *tmc2b* (accession no.
511 F1QZE9), *tomt* (accession no. A0A193KX02), *pcdh15a* (accession no. Q5ICW6), *lhfpl5a*
512 (accession no. F1Q837), *actba* (accession no. Q7ZVI7).

513

514 **Transgenic lines and plasmid construction**

515 The following previously published transgenic lines were used: *Tg(-6myo6b:β-actin-*
516 *GFP-pA)* [34], *Tg(-6myo6b:pcdh15aCD3-mEGFP-pA)* [17], and *Tg(-6myo6b:GFP-lhfpl5a-pA),*
517 *Tg(-6myo6b:Tmc1-mEGFP-pA), Tg(-6myo6b:Tmc2b-mEGFP-pA)* [11].

518 To generate the *tmie* expression vectors, we used the Tol2/Gateway system [45]. The
519 pDestination vector contained either a *cmlc2:GFP* heart marker or α-*ACry:mCherry* eye marker
520 for sorting. pDESTtol2pACrymCherry was a gift from Joachim Berger and Peter Currie
521 (Addgene plasmid # 64023, [46]).

522 The 5' entry vector contained the promoter for the *myosin 6b* gene, which drives
523 expression only in hair cells. All *tmie* transgenic constructs were subcloned into the middle entry
524 vector using PCR or bridging PCR and confirmed by sequencing. The primers for each vector
525 are listed in Table 1. For GFP-tagging, we used a 3' entry vector with a flexible linker
526 (GHGTGSTGSGSS) followed by *emEGFP*. For *NLS(mCherry)* experiments, a p2A self-
527 cleaving peptide (GSGATNFSLLKQAGDVEENPGP) was interposed between the *tmie*
528 construct and the *NLS(mCherry)*. This causes translation of a fusion protein that is subsequently
529 cleaved into the two final proteins. The 2TM helix replacements from residues 21-43 result in the
530 following chimeric helices: CD8 (YIWAPLAGTCGVLLLSLVITLYC), CD8-2TM
531 (YIWAPLAGTCGILAIIITLCCIF), and 2TM-CD8 (LWQVVGIFSMFVLLLSLVITLYC).

532 Multisite Gateway LR reactions [47, 48] were performed to generate the following
533 constructs: *pDest(-6myo6b:tmie-GFP-pA)*, *pDest(-6myo6b:tmie-short-GFP-pA), pDest(-*
534 *6myo6b:SP44-231-GFP-pA), pDest(-6myo6b:SP63-231-GFP-pA), pDest(-6myo6b:Δ63-73-*
535 *GFP-pA), pDest(-6myo6b:CD8-GFP-pA), pDest(-6myo6b:CD8-2TM-GFP-pA), pDest(-*
536 *6myo6b:2TM-CD8-GFP-pA), pDest(-6myo6b:Δ97-113-GFP-pA), pDest(-6myo6b:Δ114-138-*

537 *GFP-pA), pDest(-6myo6b:1-113-GFP-pA), pDest(-6myo6b:1-138-GFP-pA), pDest(-*
538 *6myo6b:tmie-p2A-NLS(mCherry)-pA), pDest(-6myo6b:SP63-231-p2A-NLS(mCherry)-pA),*
539 *pDest(-6myo6b:Δ63-73-p2A-NLS(mCherry)-pA), pDest(-6myo6b:CD8-2TM-p2A-*
540 *NLS(mCherry)-pA), pDest(-6myo6b:Δ97-113-p2A-NLS(mCherry)-pA).*

541 To generate transgenic fish, plasmid DNA and *tol2* transposase mRNA were co-injected
542 into single-cell fertilized eggs, as previously described (Kwan et al., 2007). For each construct,
543 200+ eggs from an incross of *tmie*^{ru1000} heterozygotes were injected. To obtain stable transgenic
544 lines, >24 larvae with strong marker expression were raised as potential founders. For each GFP-
545 tagged transgene, at least two founder lines were generated and examined for visible bundle
546 expression. For each *tmie* construct, we isolated a line containing single transgene insertions,
547 with the exception of the *CD8-2TM* construct in which we identified a single founder with high
548 transmission of the transgene (>10%) and used these offspring and their siblings for FM and
549 microphonics experiments. For *NLS(mCherry)* experiments, injected fish were raised to
550 adulthood and genotyped to identify *tmie*^{ru1000} heterozygotes and homozygotes. We identified
551 founders for each construct and then crossed these founders to *tmie*^{ru1000} heterozygotes carrying
552 *Tg(myo6b:tmc2b-GFP)*. This generated offspring that expressed both transgenes in the *tmie*^{ru1000}
553 mutant background, and we used these larvae for experiments. In *SP44-231*, *SP63-231*, and
554 *CD8-2TM*, stable transgenic lines were generated from the founder before experiments were
555 carried out.
556

557 **Microscopy**

558 Live larvae were anesthetized with E3 plus 0.03% 3-amino benzoic acid ethylester
559 (MESAB; Western Chemical) and mounted in 1.5% low-melting-point agarose (Sigma-Aldrich

560 cas. # 39346-81-1), with the exception of the morphology images from Fig 1A and Fig 6A in
561 which larvae were pinned with glass rods and imaged in E3 or extracellular solution containing
562 MESAB. The image in Fig 6A was captured at room temperature using a Hamamatsu digital
563 camera (C11440, ORCA-flash2.8), MetaMorph Advanced NX software, and an upright Leica
564 DMLFS microscope. We used differential interference contrast (DIC) with a Leica HC PL
565 Fluotar 10x/0.3 lens. For all imaging except Fig 6A, images were captured at room temperature
566 using an Axiocam MrM camera, Zeiss Zen software, and an upright Zeiss LSM700 laser-
567 scanning confocal microscope. We used DIC with one of two water-immersion lenses: Plan
568 Apochromat 40x/1.0 DIC, or Acroplan 63x/0.95 W. Laser power and gain were unique for each
569 fluorophore to prevent photobleaching. We averaged 2 or 4x for each image, consistent within
570 each experiment. The Tmc1-GFP and Tmc2b-GFP transgenes are very dim, and high laser power
571 (4%) and gain (1100) were necessary. At these settings, autofluorescence from other
572 wavelengths can falsely enhance the emission peak at 488. To filter out this autofluorescence, we
573 simultaneously collected light on a second channel with an emission peak at 640 nm.
574

575 **Auditory Evoked Behavioral Response (AEBR)**

576 Experiments were conducted as previously described [49]. Wild type and mutant larvae
577 were sorted by FM 1-43 labeling. Briefly, 6 dpf larvae were placed in six central wells of a 96-
578 well microplate mounted on an audio speaker. Pure tones were played every 15 s for 3 min
579 (twelve 100 ms stimuli at 1 kHz, sound pressure level 157 dB, denoted by asterisks in Fig 1B).
580 Responses were recorded in the dark inside a Zebrabox monitoring system (ViewPoint Life
581 Sciences). Peaks represent pixel changes from larval movement. A response was considered
582 positive if it occurred within two seconds after the stimulus and surpassed threshold to be

583 considered evoked, not spontaneous (Fig 1B, green indicates movement detected, magenta
584 indicates threshold surpassed). For each larva, we used the best response rate out of three trials.
585 Response was quantified by dividing the number of positive responses by total stimuli (12) and
586 converting to a percent. If the larvae moved within two seconds before a stimulus, that stimulus
587 was dropped from the trial data set (i.e. the number of total stimuli would become 11). Each data
588 point on the graph in Fig 1C is the percent response of an individual larva. We used a two-tailed
589 unpaired t-test with Welch's correction to determine significance, ****$p<0.0001$.
590

591 **FM 1-43 and FM 4-64 labeling**

592 Larvae were briefly exposed to E3 containing either 3µM N-(3-
593 Triethylammoniumpropyl)-4-(4-(Dibutylamino)styryl)Pyridinium Dibromide (FM 1-43, Life
594 Technologies) or 3µM of the red-shifted *N[scap]*-(3-triethylammoniumpropyl)-4-(6-(4-
595 (diethylamino)phenyl)hexatrienyl)pyridinium dibromide (FM4-64; Invitrogen). After exposure
596 for 25-30 seconds, larvae were washed 3x in E3. Laser power was adjusted for each experiment
597 to avoid saturation of pixels but was consistent within a clutch. FM levels were quantified in
598 ImageJ [50] as described previously [9]. In brief, maximum projections of each neuromast were
599 generated using seven optical sections, beginning at the cuticular plate and moving down through
600 the soma (magenta bracket, Fig 1G). We then measured the integrated density of the channel
601 with an emission peak at 640 nm for FM 4-64, and at 488 nm for FM 1-43. This integrated
602 density value was divided by the number of cells, thus converting each neuromast into a single
603 plot point of integrated density per cell (IntDens/cell). Statistical analyses were always
604 performed between direct siblings. For Fig 5, individual values were divided by the mean of the
605 sibling wild type neuromasts in order to display the data as a percent of wild type, making it

606 easier to compare across groups. Statistical significance was determined within an individual
607 clutch using one-way ANOVA.
608
609 **Microphonics**
610 Larvae at 3 dpf were anesthetized in extracellular solution (140mM NaCl, 2mM KCl,
611 2mM $CaCl_2$, 1mM $MgCl_2$, and 10mM 4-(2-hydroxyethyl)-1-piperazineethanesulfonic acid
612 (HEPES); pH 7.4) containing 0.02% 3-amino benzoic acid ethylester (MESAB; Western
613 Chemical). Two glass fibers straddled the yolk to pin the larvae against a perpendicular cross-
614 fiber. Recording pipettes were pulled from borosilicate glass with filament, O.D.: 1.5 mm, O.D.:
615 0.86 mm, 10 cm length (Sutter, item # BF150-86-10, fire polished). Using the Sutter Puller
616 (model P-97), we pulled the pipettes into a long shank with a resistance of 10-20MΩ. We then
617 used a Sutter Beveler with impedance meter (model BV-10C) to bevel the edges of the recording
618 pipettes to a resistance of 3-6 MΩ. We pulled a second pipette to a long shank and fire polished
619 to a closed bulb, and then attached this rod to a piezo actuator (shielded with tin foil). The rod
620 was then pressed to the front of the head behind the lower eye, level with the otoliths in the ear
621 of interest, to hold the head in place while the recording pipette was advanced until it pierced the
622 inner ear cover. Although it has been demonstrated that size of response is unchanged by entry
623 point [51], we maintained a consistent entry point dorsal to the anterior crista and lateral to the
624 posterior crista (see Fig 6A). After the recording pipette was situated, the piezo pipette was then
625 moved back to a position in light contact with the head. We drove the piezo with a High Power
626 Amplifier (piezosystem jena, System ENT/ENV, serial # E18605), and recorded responses in
627 current clamp mode with a patch-clamp amplifier (HEKA, EPC 10 usb double, serial # 550089).
628 Each stimulus was of 20 ms duration, with 20 ms pre- and post-stimulus periods. We used either

629 a sine wave or a voltage step and recorded at 20 kHz, collecting 200 traces per experiment. In
630 Fig 1H, we used a 200 Hz sine wave at 10V, based on reports that 200 Hz elicited the strongest
631 response [52]. In Fig 6, we used multiple step stimuli at varying voltages (2V, 3V, 4V, 5V, 6V,
632 and 10V). The piezo signal was low-pass filtered at 500Hz using the Low-Pass Bessel Filter 8
633 Pole (Warner Instruments). Microphonic potential responses were amplified 1000x and filtered
634 between 0.1-3000 Hz by the Brownlee Precision Instrumentation Amplifier (Model 440). We
635 used Igor Pro for analysis. We averaged each set of 200 traces to generate one trace response per
636 fish, then measured baseline-to-peak amplitude. These amplitudes were used to generate the
637 graphs in Fig 6. Statistical significance was determined by 2-way ANOVA comparing all groups
638 to wild type non-transgenic siblings.
639

640 **Quantification of Tg(myo6b:Tmc1-GFP) and Tg(myo6b:Tmc2b-GFP) in the ROI**

641 Using ImageJ, maximum projections of each crista were generated for analysis (5
642 sections per stack for Tmc1-GFP in Fig 3D and Tmc2b-GFP in Fig 3F, and 13 sections per stack
643 for Tmc2b-GFP in Figs 3H and 7). Quantification of Tmc-GFP bundle fluorescence in Fig 3 was
644 achieved by outlining each bundle to encompass the entire region of interest (ROI) in a single
645 hand-drawn area (Fig 7A, right panel, black outline). In the ROI, we quantified the integrated
646 density of the channel with an emission peak at 480 nm. This was repeated in the region above
647 the bundles containing only inner ear fluid and the kinocilia in order to subtract background
648 fluorescence. Each middle crista generated one data point on the graphs in Figs 3 and 7. In some
649 cases, we saw single cells that appeared to have a GFP-fill, probably due to clipping of the GFP
650 tag. We excluded these cells from analyses, since they falsely increased the signal. Due to the 3D
651 nature of the mound-shaped cristae, it was difficult to completely exclude the apical soma region,

652 leading the signals of *tmie*^{ru1000} to average above zero. We used the Kruskal-Wallis test for the
653 SP44-231, SP63-231, and 2TM-CD8 constructs; all others are one-way ANOVA.
654
655 **cDNA generation by Reverse Transcription Polymerase Chain Reaction (RT-PCR)**
656 We sorted 30 wild type and 30 *t26171* larvae by behavior (tap sensitivity and balance
657 defect at 5 dpf) and extracted RNA using the RNeasy mini kit (Qiagen). Larvae were
658 homogenized using a 1ml syringe. To generate the cDNA for the short isoform of Tmie (Tmie-
659 short) and the t26171 allele, we performed RT-PCR on these RNA samples using the RNA to
660 cDNA EcoDry Premix (Clontech, Cat # 639549). Primers are listed in Table 1. Both transcripts
661 were verified by DNA sequencing.
662

663 ## Acknowledgements
664 The authors thank Cecilia Toro, Lucille Moore, and Andre Dagostin for help with
665 execution and analysis of the microphonics experiments, as well as Larry Trussell, Josef Trapani,
666 and Anthony Ricci for advice. We thank Jim Hudspeth for the *tmie*^{ru1000} fish line. We also thank
667 Eliot Smith for feedback on the manuscript, and Leah Snyder and Lisa Hiyashi for laboratory
668 support.

669 ## References
670 1. Kozlov AS, Risler T, Hudspeth AJ. Coherent motion of stereocilia assures the concerted
671 gating of hair-cell transduction channels. Nature neuroscience. 2007;10(1):87-92.

672 2. Beurg M, Fettiplace R, Nam JH, Ricci AJ. Localization of inner hair cell
673 mechanotransducer channels using high-speed calcium imaging. Nature neuroscience.
674 2009;12(5):553-8.
675 3. Kurima K, Ebrahim S, Pan B, Sedlacek M, Sengupta P, Millis BA, et al. TMC1 and
676 TMC2 Localize at the Site of Mechanotransduction in Mammalian Inner Ear Hair Cell
677 Stereocilia. Cell reports. 2015;12(10):1606-17.
678 4. Hudspeth AJ. How the ear's works work. Nature. 1989;341(6241):397-404.
679 5. Kurima K, Peters LM, Yang Y, Riazuddin S, Ahmed ZM, Naz S, et al. Dominant and
680 recessive deafness caused by mutations of a novel gene, TMC1, required for cochlear hair-cell
681 function. Nature genetics. 2002;30(3):277-84.
682 6. Kawashima Y, Geleoc GS, Kurima K, Labay V, Lelli A, Asai Y, et al.
683 Mechanotransduction in mouse inner ear hair cells requires transmembrane channel-like genes.
684 The Journal of clinical investigation. 2011;121(12):4796-809.
685 7. Pan B, Geleoc GS, Asai Y, Horwitz GC, Kurima K, Ishikawa K, et al. TMC1 and TMC2
686 are components of the mechanotransduction channel in hair cells of the mammalian inner ear.
687 Neuron. 2013;79(3):504-15.
688 8. Beurg M, Xiong W, Zhao B, Muller U, Fettiplace R. Subunit determination of the
689 conductance of hair-cell mechanotransducer channels. Proceedings of the National Academy of
690 Sciences of the United States of America. 2015;112(5):1589-94.
691 9. Maeda R, Kindt KS, Mo W, Morgan CP, Erickson T, Zhao H, et al. Tip-link protein
692 protocadherin 15 interacts with transmembrane channel-like proteins TMC1 and TMC2.
693 Proceedings of the National Academy of Sciences of the United States of America.
694 2014;111(35):12907-12.

695 10. Chou SW, Chen Z, Zhu S, Davis RW, Hu J, Liu L, et al. A molecular basis for water
696 motion detection by the mechanosensory lateral line of zebrafish. Nature communications.
697 2017;8(1):2234.
698 11. Erickson T, Morgan CP, Olt J, Hardy K, Busch-Nentwich E, Maeda R, et al. Integration
699 of Tmc1/2 into the mechanotransduction complex in zebrafish hair cells is regulated by
700 Transmembrane O-methyltransferase (Tomt). eLife. 2017;6.
701 12. Beurg M, Cui R, Goldring AC, Ebrahim S, Fettiplace R, Kachar B. Variable number of
702 TMC1-dependent mechanotransducer channels underlie tonotopic conductance gradients in the
703 cochlea. Nature communications. 2018;9(1):2185.
704 13. Corns LF, Johnson SL, Kros CJ, Marcotti W. Tmc1 Point Mutation Affects Ca2+
705 Sensitivity and Block by Dihydrostreptomycin of the Mechanoelectrical Transducer Current of
706 Mouse Outer Hair Cells. The Journal of neuroscience : the official journal of the Society for
707 Neuroscience. 2016;36(2):336-49.
708 14. Corns LF, Jeng JY, Richardson GP, Kros CJ, Marcotti W. TMC2 Modifies Permeation
709 Properties of the Mechanoelectrical Transducer Channel in Early Postnatal Mouse Cochlear
710 Outer Hair Cells. Frontiers in molecular neuroscience. 2017;10:326.
711 15. Indzhykulian AA, Stepanyan R, Nelina A, Spinelli KJ, Ahmed ZM, Belyantseva IA, et al.
712 Molecular remodeling of tip links underlies mechanosensory regeneration in auditory hair cells.
713 PLoS biology. 2013;11(6):e1001583.
714 16. Kazmierczak P, Sakaguchi H, Tokita J, Wilson-Kubalek EM, Milligan RA, Muller U, et
715 al. Cadherin 23 and protocadherin 15 interact to form tip-link filaments in sensory hair cells.
716 Nature. 2007;449(7158):87-91.

717 17. Maeda R, Pacentine IV, Erickson T, Nicolson T. Functional Analysis of the
718 Transmembrane and Cytoplasmic Domains of Pcdh15a in Zebrafish Hair Cells. The Journal of
719 neuroscience : the official journal of the Society for Neuroscience. 2017;37(12):3231-45.
720 18. Xiong W, Grillet N, Elledge HM, Wagner TF, Zhao B, Johnson KR, et al. TMHS is an
721 integral component of the mechanotransduction machinery of cochlear hair cells. Cell.
722 2012;151(6):1283-95.
723 19. Giese APJ, Tang YQ, Sinha GP, Bowl MR, Goldring AC, Parker A, et al. CIB2 interacts
724 with TMC1 and TMC2 and is essential for mechanotransduction in auditory hair cells. Nature
725 communications. 2017;8(1):43.
726 20. Mitchem KL, Hibbard E, Beyer LA, Bosom K, Dootz GA, Dolan DF, et al. Mutation of
727 the novel gene Tmie results in sensory cell defects in the inner ear of spinner, a mouse model of
728 human hearing loss DFNB6. Human molecular genetics. 2002;11(16):1887-98.
729 21. Gleason MR, Nagiel A, Jamet S, Vologodskaia M, Lopez-Schier H, Hudspeth AJ. The
730 transmembrane inner ear (Tmie) protein is essential for normal hearing and balance in the
731 zebrafish. Proceedings of the National Academy of Sciences of the United States of America.
732 2009;106(50):21347-52.
733 22. Shen YC, Jeyabalan AK, Wu KL, Hunker KL, Kohrman DC, Thompson DL, et al. The
734 transmembrane inner ear (tmie) gene contributes to vestibular and lateral line development and
735 function in the zebrafish (Danio rerio). Dev Dyn. 2008;237(4):941-52.
736 23. Naz S, Giguere CM, Kohrman DC, Mitchem KL, Riazuddin S, Morell RJ, et al.
737 Mutations in a novel gene, TMIE, are associated with hearing loss linked to the DFNB6 locus.
738 American journal of human genetics. 2002;71(3):632-6.

739 24. Cho KI, Suh JG, Lee JW, Hong SH, Kang TC, Oh YS, et al. The circling mouse
740 (C57BL/6J-cir) has a 40-kilobase genomic deletion that includes the transmembrane inner ear
741 (tmie) gene. Comparative medicine. 2006;56(6):476-81.
742 25. Zhao B, Wu Z, Grillet N, Yan L, Xiong W, Harkins-Perry S, et al. TMIE is an essential
743 component of the mechanotransduction machinery of cochlear hair cells. Neuron.
744 2014;84(5):954-67.
745 26. Park S, Lee JH, Cho HJ, Lee KY, Kim MO, Yun BW, et al. tmie Is required for
746 gentamicin uptake by the hair cells of mice. Comparative medicine. 2013;63(2):136-42.
747 27. Gale JE, Marcotti W, Kennedy HJ, Kros CJ, Richardson GP. FM1-43 dye behaves as a
748 permeant blocker of the hair-cell mechanotransducer channel. The Journal of neuroscience : the
749 official journal of the Society for Neuroscience. 2001;21(18):7013-25.
750 28. Meyers JR, MacDonald RB, Duggan A, Lenzi D, Standaert DG, Corwin JT, et al.
751 Lighting up the senses: FM1-43 loading of sensory cells through nonselective ion channels. The
752 Journal of neuroscience : the official journal of the Society for Neuroscience. 2003;23(10):4054-
753 65.
754 29. Shin MJ, Lee JH, Yu DH, Kim HJ, Bae KB, Yuh HS, et al. Spatiotemporal expression of
755 tmie in the inner ear of rats during postnatal development. Comparative medicine.
756 2010;60(4):288-94.
757 30. Su MC, Yang JJ, Chou MY, Hsin CH, Su CC, Li SY. Expression and localization of
758 Tmie in adult rat cochlea. Histochemistry and cell biology. 2008;130(1):119-26.
759 31. Webb SW, Grillet N, Andrade LR, Xiong W, Swarthout L, Della Santina CC, et al.
760 Regulation of PCDH15 function in mechanosensory hair cells by alternative splicing of the
761 cytoplasmic domain. Development (Cambridge, England). 2011;138(8):1607-17.

762 32. Seiler C, Finger-Baier KC, Rinner O, Makhankov YV, Schwarz H, Neuhauss SC, et al.
763 Duplicated genes with split functions: independent roles of protocadherin15 orthologues in
764 zebrafish hearing and vision. Development (Cambridge, England). 2005;132(3):615-23.
765 33. Clemens Grisham R, Kindt K, Finger-Baier K, Schmid B, Nicolson T. Mutations in
766 ap1b1 cause mistargeting of the Na(+)/K(+)-ATPase pump in sensory hair cells. PloS one.
767 2013;8(4):e60866.
768 34. Kindt KS, Finch G, Nicolson T. Kinocilia mediate mechanosensitivity in developing
769 zebrafish hair cells. Developmental cell. 2012;23(2):329-41.
770 35. Cunningham CL, Wu Z, Jafari A, Zhao B, Schrode K, Harkins-Perry S, et al. The murine
771 catecholamine methyltransferase mTOMT is essential for mechanotransduction by cochlear hair
772 cells. eLife. 2017;6.
773 36. Karuppasamy S, Nam YY, Jung H, Suh JG. Expression of deafness protein Tmie in
774 postnatal developmental stages of C57BL/6J mice. Laboratory Animal Research.
775 2012;28(2):147-50.
776 37. Shin MJ, Lee JH, Yu DH, Kim BS, Kim HJ, Kim SH, et al. Ectopic expression of tmie
777 transgene induces various recovery levels of behavior and hearing ability in the circling mouse.
778 Biochemical and biophysical research communications. 2008;374(1):17-21.
779 38. Mahendrasingam S, Fettiplace R, Alagramam KN, Cross E, Furness DN. Spatiotemporal
780 changes in the distribution of LHFPL5 in mice cochlear hair bundles during development and in
781 the absence of PCDH15. PloS one. 2017;12(10):e0185285.
782 39. Senften M, Schwander M, Kazmierczak P, Lillo C, Shin JB, Hasson T, et al. Physical and
783 functional interaction between protocadherin 15 and myosin VIIa in mechanosensory hair cells.

784 The Journal of neuroscience : the official journal of the Society for Neuroscience.
785 2006;26(7):2060-71.
786 40. Kall L, Krogh A, Sonnhammer EL. A combined transmembrane topology and signal
787 peptide prediction method. Journal of molecular biology. 2004;338(5):1027-36.
788 41. Ganapathy A, Pandey N, Srisailapathy CR, Jalvi R, Malhotra V, Venkatappa M, et al.
789 Non-syndromic hearing impairment in India: high allelic heterogeneity among mutations in
790 TMPRSS3, TMC1, USHIC, CDH23 and TMIE. PloS one. 2014;9(1):e84773.
791 42. Santos RL, El-Shanti H, Sikandar S, Lee K, Bhatti A, Yan K, et al. Novel sequence
792 variants in the TMIE gene in families with autosomal recessive nonsyndromic hearing
793 impairment. Journal of molecular medicine (Berlin, Germany). 2006;84(3):226-31.
794 43. Sirmaci A, Ozturkmen-Akay H, Erbek S, Incesulu A, Duman D, Tasir-Yilmaz S, et al. A
795 founder TMIE mutation is a frequent cause of hearing loss in southeastern Anatolia. Clinical
796 genetics. 2009;75(6):562-7.
797 44. Obholzer N, Wolfson S, Trapani JG, Mo W, Nechiporuk A, Busch-Nentwich E, et al.
798 Vesicular glutamate transporter 3 is required for synaptic transmission in zebrafish hair cells.
799 The Journal of neuroscience : the official journal of the Society for Neuroscience.
800 2008;28(9):2110-8.
801 45. Kwan KM, Fujimoto E, Grabher C, Mangum BD, Hardy ME, Campbell DS, et al. The
802 Tol2kit: a multisite gateway-based construction kit for Tol2 transposon transgenesis constructs.
803 Developmental dynamics : an official publication of the American Association of Anatomists.
804 2007;236(11):3088-99.
805 46. Berger J, Currie PD. 503unc, a small and muscle-specific zebrafish promoter. Genesis
806 (New York, NY : 2000). 2013;51(6):443-7.

807 47. Hartley JL, Temple GF, Brasch MA. DNA cloning using in vitro site-specific
808 recombination. Genome research. 2000;10(11):1788-95.
809 48. Cheo DL, Titus SA, Byrd DR, Hartley JL, Temple GF, Brasch MA. Concerted assembly
810 and cloning of multiple DNA segments using in vitro site-specific recombination: functional
811 analysis of multi-segment expression clones. Genome research. 2004;14(10b):2111-20.
812 49. Einhorn Z, Trapani JG, Liu Q, Nicolson T. Rabconnectin3alpha promotes stable activity
813 of the H+ pump on synaptic vesicles in hair cells. The Journal of neuroscience : the official
814 journal of the Society for Neuroscience. 2012;32(32):11144-56.
815 50. Schneider CA, Rasband WS, Eliceiri KW. NIH Image to ImageJ: 25 years of image
816 analysis. Nature methods. 2012;9(7):671-5.
817 51. Tanimoto M, Ota Y, Inoue M, Oda Y. Origin of inner ear hair cells: morphological and
818 functional differentiation from ciliary cells into hair cells in zebrafish inner ear. The Journal of
819 neuroscience : the official journal of the Society for Neuroscience. 2011;31(10):3784-94.
820 52. Lu Z, DeSmidt AA. Early development of hearing in zebrafish. Journal of the
821 Association for Research in Otolaryngology : JARO. 2013;14(4):509-21.
822
823
824 **Fig Legends**
825
826 **Fig 1. Zebrafish *tmie*^{ru1000} mutants: phenotype and functional rescue by Tmie-GFP.** All
827 confocal images are of live, anesthetized larvae. (A) Hair cells in the lateral-line neuromasts (7
828 dpf) and inner ear cristae (5 dpf) from wild type and *tmie*^{ru1000} larvae. A transgene (Actin-GFP)
829 was used to visualize stereocilia bundles. (B) Sample traces from an auditory evoked behavior

830 response (AEBR) assay, performed on 6 dpf larvae over the course of 3 minutes. Pure tone
831 stimuli are indicated by asterisks. Peaks represent pixel changes due to larval movements
832 (magenta indicates positive response). (C) Quantification of AEBR displayed as box-and-
833 whiskers plot; significance determined by unpaired t-test with Welch's correction. (D) Top-down
834 view of neuromasts from 4 dpf larvae after brief exposure to a vital dye, FM 1-43. FM 1-43 and
835 FM4-64 permeate open transduction channels. (E) Lateral view of a neuromast from a 4 dpf
836 *tmie*^{ru1000} larva expressing transgenic Tmie-GFP, after exposure to FM 4-64. (F) Quantification
837 of FM 4-64 fluorescence/cell in 5 dpf larvae; significance determined by one-way ANOVA. (G)
838 A cartoon depiction of a group of lateral-line hair cells viewed laterally, with close-up views of a
839 single cell at the bundle region. The dashed green line indicates the single plane containing the
840 stereocilia bundles. The magenta bracket indicates the area used to make the maximum
841 projections that were analyzed for FM fluorescence in (F). (H) Sample traces of extracellular
842 (microphonic) recordings, evoked from the inner ear of 3 dpf larvae. A piezo actuator was used
843 to stimulate larvae with a 200 Hz sine-wave mechanical stimulus using an 8 V driver voltage. All
844 statistics are mean ± SD, ****$p<0.0001$. Scale bars: 10µm.
845
846 **Fig 2. Tmie-GFP is present in the hair bundles of MET mutants.** Confocal images of the
847 bundle region in hair cells of the inner-ear lateral crista in live larvae. Larvae at 6 dpf expressing
848 transgenic Tmie-GFP in the genetic backgrounds of wild type (A), and homozygous mutants for
849 the tip link protein Pcdh15a (B, *pcdh15a*^{psi7}), the accessory protein Lhfpl5a (C, *lhfpl5a*^{tm290d}), and
850 the Golgi-localized protein Tomt (D, *tomt*^{tk256c}). Tomt-deficient fish lack Tmc expression in hair
851 cell bundles [11], presumably mimicking the condition of a triple Tmc knockout. Arrowheads
852 indicate splayed hair bundles. n=8 each genotype. Scale bar: 5µm.

853

854 **Fig 3. Specific loss of Tmc1 and Tmc2b in tmieru1000 larvae.** Maximum projections of the
855 hair bundle region (ROI) of hair cells in the lateral crista of the inner ear, collected from live
856 larvae using confocal microscopy. (A-B) 6 dpf larvae expressing either transgenic Pcdh15aCD3-
857 GFP or GFP-Lhfpl5a (n=6 each genotype). (C) 3 dpf larvae expressing Tmc1-GFP. (D) Plot of
858 the integrated density of Tmc1-GFP fluorescence in the ROI; each data point represents one
859 crista. Statistical significance determined by two-tailed unpaired t-test with Welch's correction,
860 p=0.0002. (E) 4 dpf larvae expressing Tmc2b-GFP. The arrow points to the cuticular plate/apical
861 soma region, just below the ROI. (F) Plot of the integrated density of Tmc2b-GFP fluorescence
862 in the ROI. Statistical significance determined by two-tailed unpaired t-test with Welch's
863 correction, p=0.0005. (G) 4 dpf *tmie*^{ru1000} larva co-expressing two transgenes, *tmc2b-GFP* and
864 *tmie-p2A-NLS(mCherry)*. The p2A linker is a self-cleaving peptide that results in equimolar
865 expression of Tmie and nuclear mCherry. (H) Plot of the integrated density of Tmc2b-GFP
866 fluorescence/crista in the ROI; significance determined by one-way ANOVA. All statistics are
867 mean ± SD. Scale bars: 5µm.

868

869 **Fig 4. Schema for a systematic domain analysis of Tmie and subcellular localization of**
870 **Tmie constructs.** (A) A linear diagram of 12 unique constructs of tmie used in our experiments.
871 Full-length Tmie is predicted to contain two hydrophobic helices or transmembrane domains
872 (1TM and 2TM). SP44-231 and SP63-231 replace part of the N-terminus with a signal peptide
873 (SP) from the Glutamate receptor 2a (in blue). In the CD8, CD8-2TM, and 2TM-CD8 constructs,
874 all or part of the 2TM is replaced by the helix from the CD8 glycoprotein (in yellow). Tmie-short
875 is a fish-specific isoform of Tmie that contains an alternate final exon (in orange). Dotted lines

876 represent internal deletions. (B) Representative confocal images of each construct being
877 expressed as a GFP-tagged transgene in hair cells of 4-6 dpf *tmie*^{ru1000} larvae. Expression is
878 mosaic due to random genomic insertion into subsets of progenitor cells after single-cell
879 injection. The expression of the CD8 construct is shown in a neuromast, while all others are in
880 the inner ear middle crista. (C) The localization of each GFP fusion protein was determined by
881 measuring the fluorescence/area in the bundle (b) and soma (s), and then calculating b/(b+s). (D)
882 Enrichment in the hair bundle is displayed as a ratio for each construct, with 1 being completely
883 bundle-enriched and 0 being completely soma-enriched. Scale bar in (B): 5µm.
884
885 **Fig 5. The second transmembrane and adjacent residues of Tmie are required for rescue of**
886 **FM labeling.** All images are a top-down view of a representative neuromast from 6 dpf larvae
887 collected using confocal microscopy. The left image is a single plane through the stereocilia
888 (green dashed line in Fig 1G) with DIC + GFP fluorescence. The right image is a maximum
889 projection of the soma region (magenta bracket in Fig 1G) showing FM 4-64 fluorescence. (A)
890 Representative images of neuromasts in *tmie*^{ru1000} larvae, each stably expressing an individual
891 tmie construct. FM fluorescence was normalized to wild type non-transgenic larvae generated
892 with the Tmie-GFP line. (B) Box-and-whiskers plot of the integrated density of FM
893 fluorescence/cell in transgenic *tmie*^{ru1000} compared to non-transgenic wild type and mutant
894 siblings for each construct. (C) Representative images of neuromasts in wild type larvae with or
895 without transgene. FM fluorescence was normalized to wild type non-transgenic larvae of the
896 Tmie-GFP line. (D) Box-and-whiskers plot of the integrated density of FM fluorescence/cell in
897 wild type neuromasts with and without transgene. Significance determined within each clutch by

898 one-way ANOVA, n≥9, **p<0.01, ***p<0.001, ****p<0.0001. Scale bars in (A) and (C) are
899 10µm.
900
901 **Fig 6. The second transmembrane and adjacent regions of Tmie are required for inner ear**
902 **microphonics.** (A) A DIC image of a 3 dpf larva anesthetized and pinned (glass fiber) for inner
903 ear recordings. Shown are a probe attached to a piezo actuator (piezo) pressed against the head
904 and a recording pipette pierced into the inner ear. (B) Traces from a wild type larva. A step
905 stimulus for 20ms was applied; 200 traces were averaged for each of the six piezo driver
906 voltages: 2V, 3V, 4V, 5V, 6V, and 10V. Gray box: magnification of the onset of response in
907 individual traces. (C-I) Same protocol as in (B). Mean amplitude of the response peak ± SD as a
908 function of the stimulus intensity of the driver voltage. Statistical significance determined by
909 two-way ANOVA comparing all groups to wild type non-transgenic siblings, n≥5, *p<0.05,
910 **p<0.01, ***p<0.001, ****p<0.0001. Scale bar: 100µm.
911
912 **Fig 7. Effect of transgenic Tmie constructs on Tmc2b-GFP bundle localization.** Confocal
913 images are maximum projections of representative inner-ear lateral cristae collected from 4 dpf
914 larvae. Upper panels show the bundle region, with all larvae stably expressing transgenic
915 Tmc2b-GFP (green). Lower panels show the soma region, with some larvae expressing
916 transgenic Tmie constructs tagged with p2A-NLS(mCherry). Nuclear mCherry (magenta) is a
917 marker for equimolar translation of the indicated Tmie construct. (A) Sibling wild type,
918 *tmie*^{ru1000}, and *tmie*^{ru1000} expressing full-length Tmie. For the quantification in (G), Tmc2b-GFP
919 fluorescence was measured within the ROI (right panel, black line). (B-G) *tmie*^{ru1000} larvae
920 expressing individual Tmie constructs tagged with p2A-NLS(mCherry), as labeled. The arrows

921 in (D) point to Tmc2b-GFP in immature hair bundles. (H) Plot of the integrated density of
922 Tmc2b-GFP fluorescence in the ROI, comparing *tmie*^{ru1000} larvae expressing a tmie construct
923 (magenta) to wild type (black) and *tmie*^{ru1000} (gray) siblings not expressing tmie construct.
924 Significance for SP44-231 and SP63-231 was determined by the Kruskal-Wallis test, for all other
925 tmie constructs by one-way ANOVA, n≥6, ***p<0.001, ****p<0.0001. Scale bars: 10µm.
926

927 **Fig 8. Summary of experimental results for tmie constructs and model of discrete**
928 **functional domains of Tmie.** (A) Symbols as follows: enhanced above wild type (++),
929 comparable to wild type (+), partially reduced (+/-), and severely reduced or absent (-). For
930 *dominant negative effect*, the effect is present (+) or absent (-). Blank spaces are not determined.
931 Refer to Fig 4A for details on constructs. (B) A model of the protein sequence of zebrafish Tmie.
932 Amino acids 1-43 are separated due to suspected cleavage as a signal peptide. Although shown
933 as a TM domain, it is unclear whether the first hydrophobic region forms a helix. Note that the
934 extracellular region (yellow glow) was never deleted in its entirety; SP63-231 deleted
935 QIPDPELLPTDPPKKPDPV, and Δ63-73 deleted TSETVVFWGLR. Also note that the TM
936 domain with orange lettering only had an effect on the stability of Tmie when the entire helix
937 was substituted.
938

939 ## Supporting information

940

941 **S1 Fig. Tmie-GFP shows variable expression in stereocilia.** Representative images of the
942 lateral crista in a wild type larva at 6 dpf, generated using confocal microscopy. (A) The hair
943 bundle region of hair cells expressing transgenic tmie-GFP driven by the myo6b promoter. The

944 arrow and bracket show, respectively, the short kinocilium and stereocilia bundle of an immature
945 hair cell. (B) A single hair bundle with "bundle fill" expression pattern produced by
946 overexpression of Tmie-GFP. (C) A single bundle with Tmie-GFP concentrated along the
947 beveled edge of the stereocilial staircase. (D) A single bundle with punctate expression of Tmie-
948 GFP suggestive of localization at the site of MET. Scale bar in (A): 5μm, in (D): 2μm.
949
950 **S2 Fig. Differential effects on function with a genomic mutation and a transgene mimic.** (A)
951 Data for a novel mutant allele of tmie, *t26171*. DNA: Chromatographs of the DNA sequence of
952 tmie in wild type (above) and *tmie*^{t26171} (below) showing the genomic region where the mutation
953 occurs. An arginine is mutated to guanine in the splice acceptor (black box, above) of the final
954 exon of tmie, exon 4. The dashed black box below indicates the mutated original splice acceptor
955 site. Use of a cryptic splice acceptor (black box, below) 8 nucleotides downstream causes a
956 frameshift and an early stop codon (*). cDNA: Chromatograph of the DNA sequence from RT-
957 PCR of *tmie*^{t26171} larvae bridging exons 3 and 4. Protein: The predicted protein products, shown
958 here as a two-pass transmembrane protein. The wild type protein has many charged residues
959 (positive in light gray, negative in dark gray) that are lost in *tmie*^{t26171}. Balance: Photos of wild
960 type and *tmie*^{t26171} larvae, taken with a hand-held Canon camera. Arrow points to a larva that is
961 upside-down, displaying a classic vestibular phenotype. (B) Top-down view of a representative
962 neuromast after exposure to FM 4-64, imaged using confocal microscopy. The first panel is a
963 single plane through the soma region while the second panel is a maximum projection of 7
964 panels through the soma region, beginning at the cuticular plate (as denoted by magenta bracket
965 in Fig 1G). (C) Same as (B) except that the first panel shows the bundle region so that 1-138-
966 GFP can be visualized in bundles (as depicted by dashed green line, Fig 1G). The transgene is

967 driven by the myo6b promoter. (D) Plot of the integrated density of FM fluorescence per cell as a
968 percent of wild type siblings. Displayed wild type and *tmie*^{ru1000} data are from siblings of *Tg(1-*
969 *138-GFP); tmie*^{ru1000}, while *tmie*^{t26171} data are from a separate experiment. Statistical significance
970 determined by one-way ANOVA, ****$p<0.0001$. Scale bar: 10µm.
971
972 **S3 Fig. Functional rescue of tmieru1000 by constructs SP63-231 and 2TM-CD8 is Tmc**
973 **dose-dependent.** (A) Mean amplitude of the response peak ± SD as a function of the stimulus
974 intensity of the driver voltage, as described in Fig 6B. (B) XY plot of the amplitude of
975 microphonic response vs the integrated density of Tmc2b-GFP fluorescence in the ROI. A 10V
976 step stimulus was used to evoke microphonic potentials. The line is a linear regression, R^2=
977 0.5216. (C) Same as (A) for the 2TM-CD8 construct. (D) Same as (B) for the 2TM-CD8
978 construct, R^2= 0.7726. Measurements are from 4 dpf larvae.
979
980 **S4 Fig. In Δ63-73, Tmc2b-GFP traffics to bundles but does not maintain high expression in**
981 **mature cells.** Confocal images of single hair bundles from cells expressing transgenic Tmc2b-
982 GFP driven by the myo6b promoter. Brackets show the stereocilia bundle, which is shorter in
983 immature hair cells (white brackets) and longer in mature ones (black brackets). Larvae are 4
984 dpf. Scale bar: 2µm.

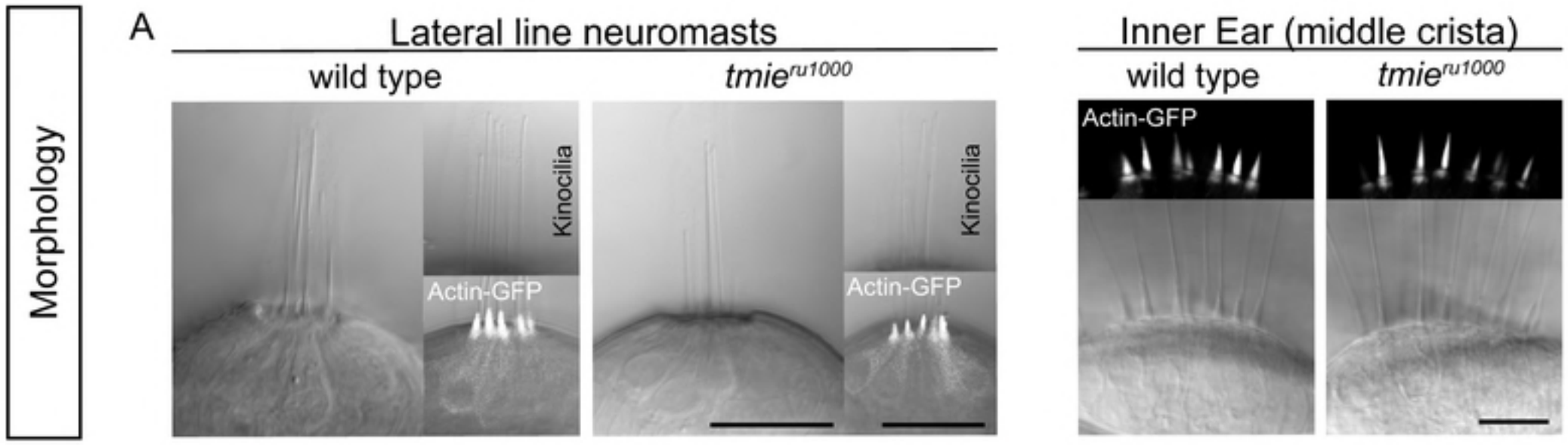
Morphology
A
Lateral line neuromasts
wild type
tmie ru1000
Kinocilia
Actin-GFP
Inner Ear (middle crista)
wild type
tmie ru1000
Actin-GFP

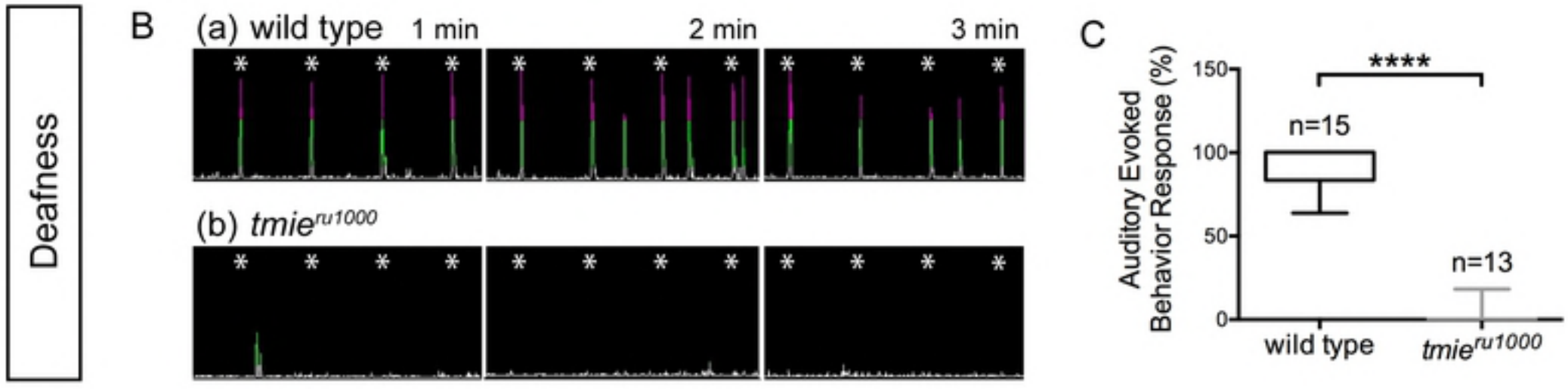
Deafness
B
(a) wild type
1 min
2 min
3 min
(b) tmie ru1000
C
Auditory Evoked Behavior Response (%)
150
100
50
0
****
n=15
n=13
wild type
tmie ru1000

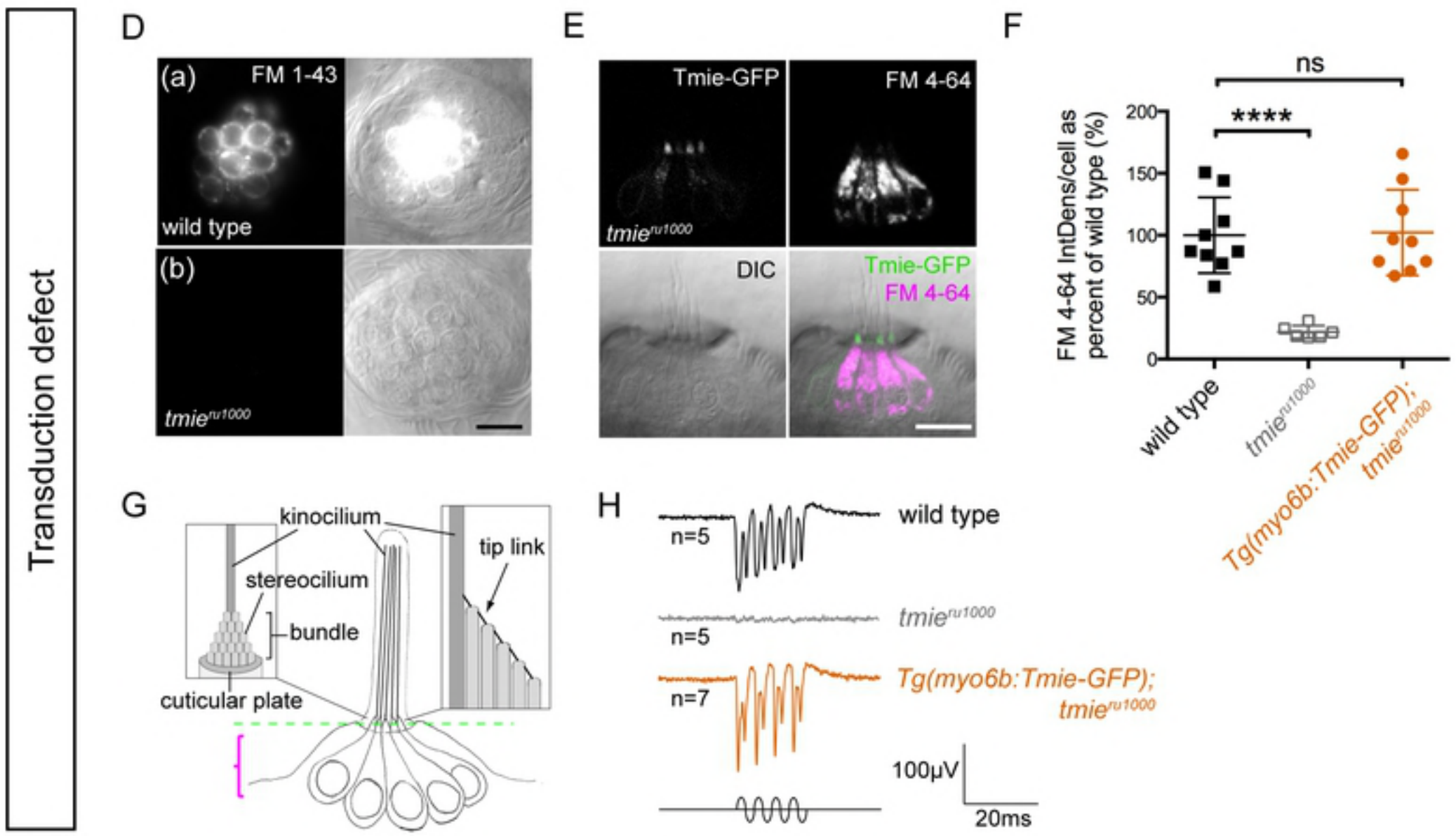
Transduction defect
D
(a)
FM 1-43
wild type
(b)
tmie ru1000
E
Tmie-GFP
FM 4-64
tmie ru1000
DIC
Tmie-GFP
FM 4-64
F
ns
****
FM 4-64 IntDens/cell as percent of wild type (%)
200
150
100
50
0
wild type
tmie ru1000
Tg(myo6b:Tmie-GFP); tmie ru1000
G
kinocilium
tip link
stereocilium
bundle
cuticular plate
H
n=5
wild type
n=5
tmie ru1000
n=7
Tg(myo6b:Tmie-GFP); tmie ru1000
100μV
20ms

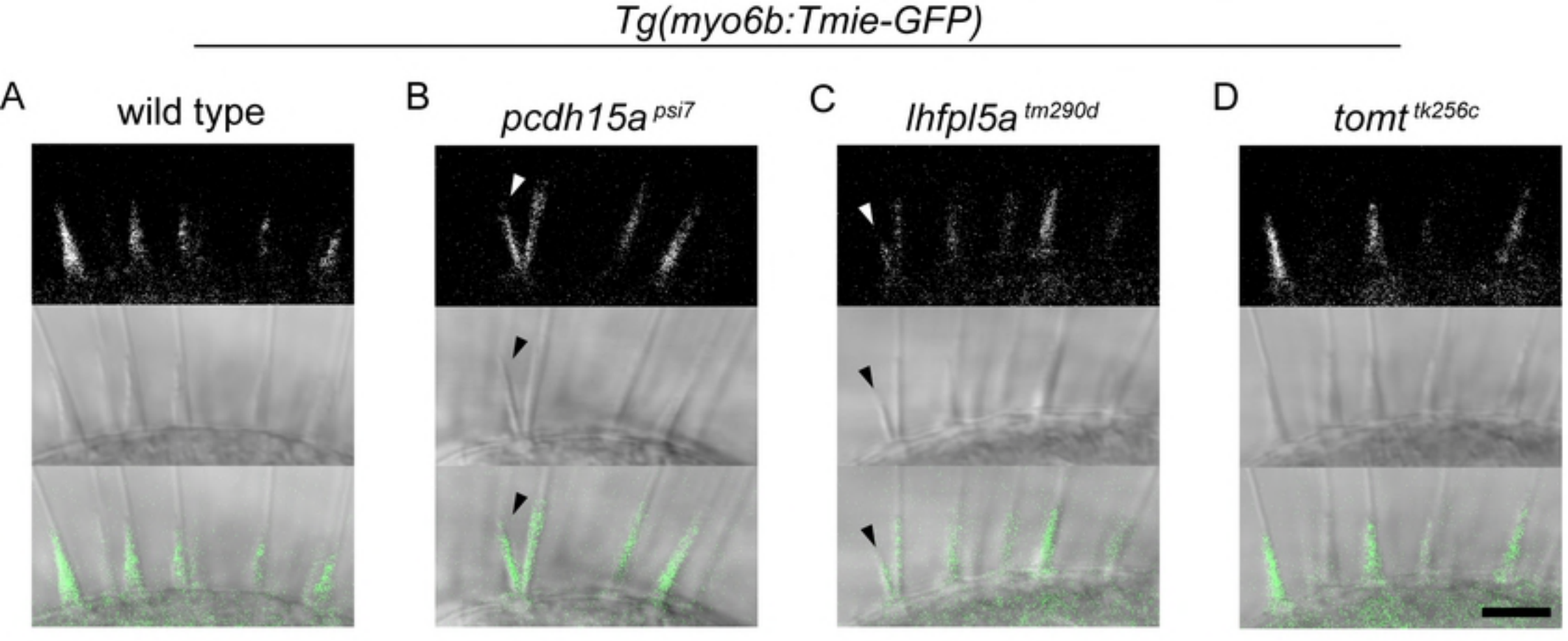
Tg(myo6b:Tmie-GFP)
A
wild type
B
pcdh15a psi7
C
lhfpl5a tm290d
D
tomt tk256c

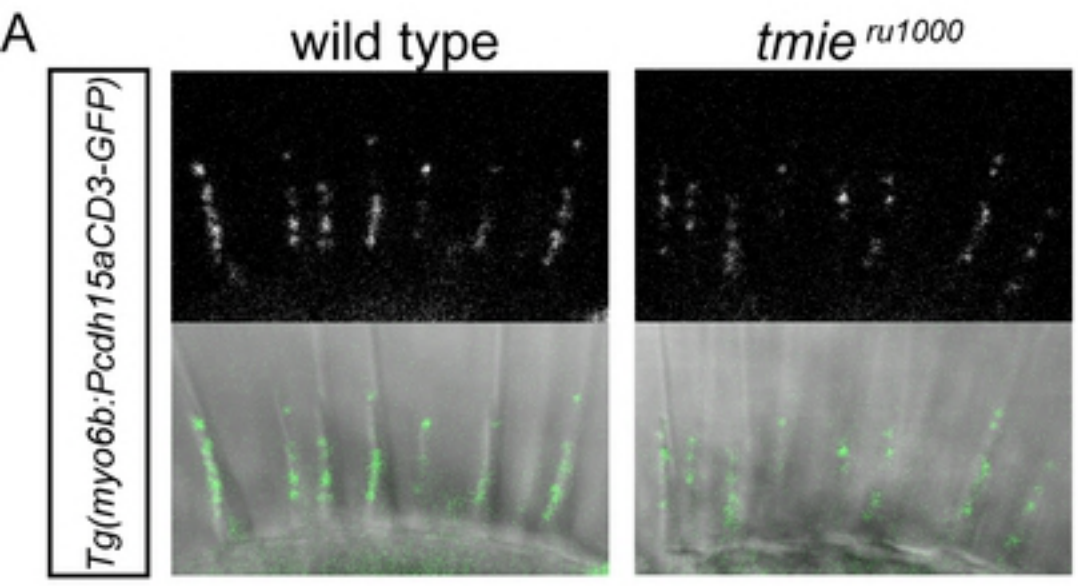
A
wild type
tmie ru1000
Tg(myo6b:Pcdh15aCD3-GFP)

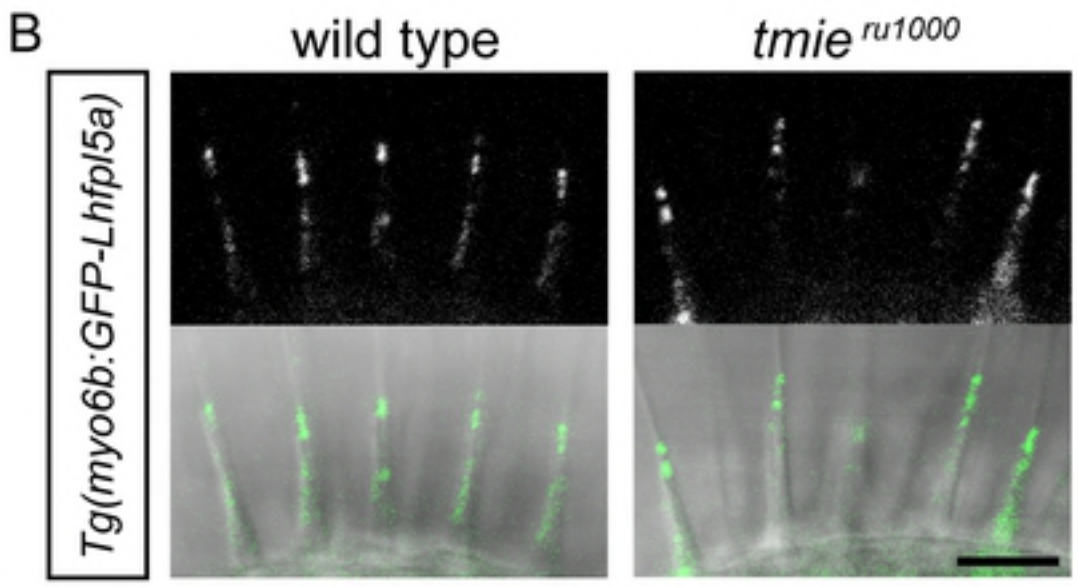
B
wild type
tmie ru1000
Tg(myo6b:GFP-Lhfpl5a)

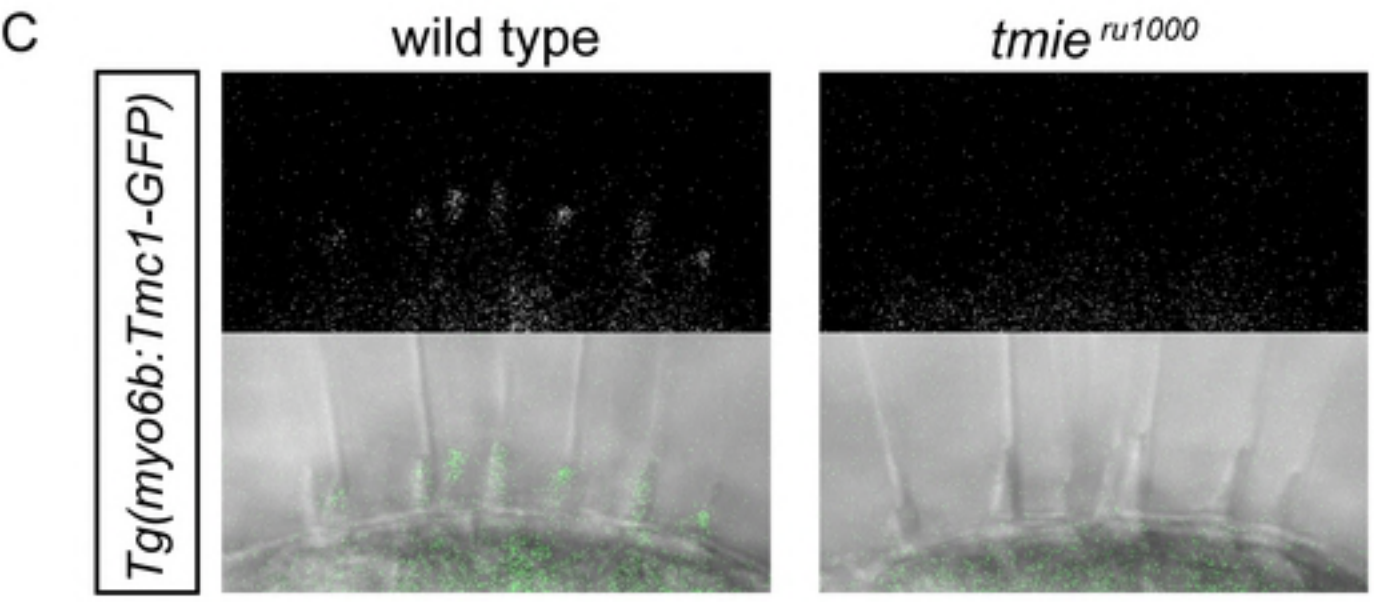
C
wild type
tmie ru1000
Tg(myo6b:Tmc1-GFP)

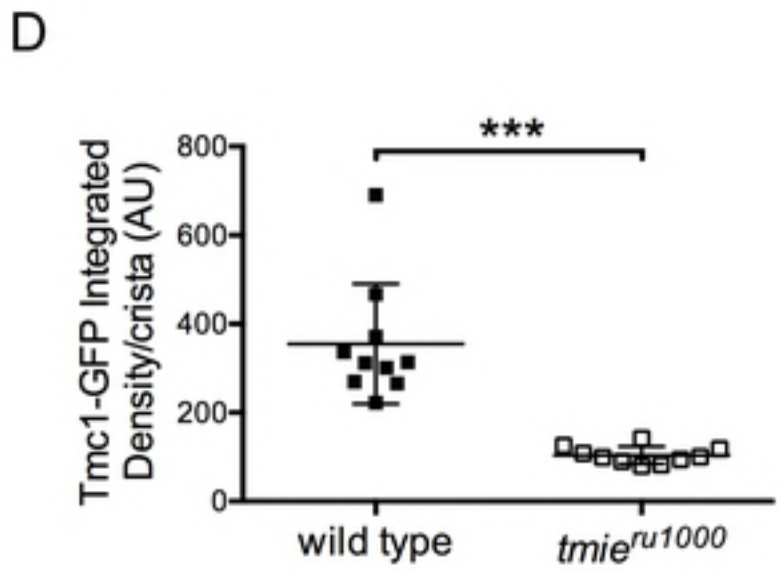
D
***
Tmc1-GFP Integrated Density/crista (AU)
800
600
400
200
0
wild type
tmie ru1000

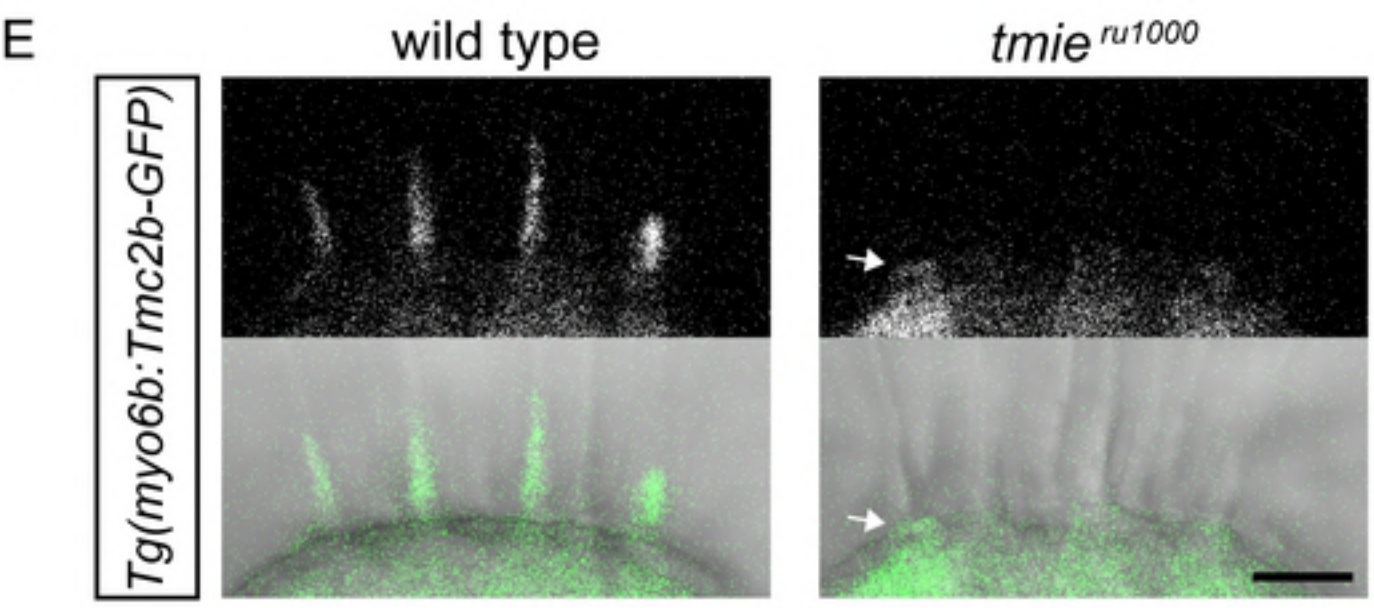
E
wild type
tmie ru1000
Tg(myo6b:Tmc2b-GFP)

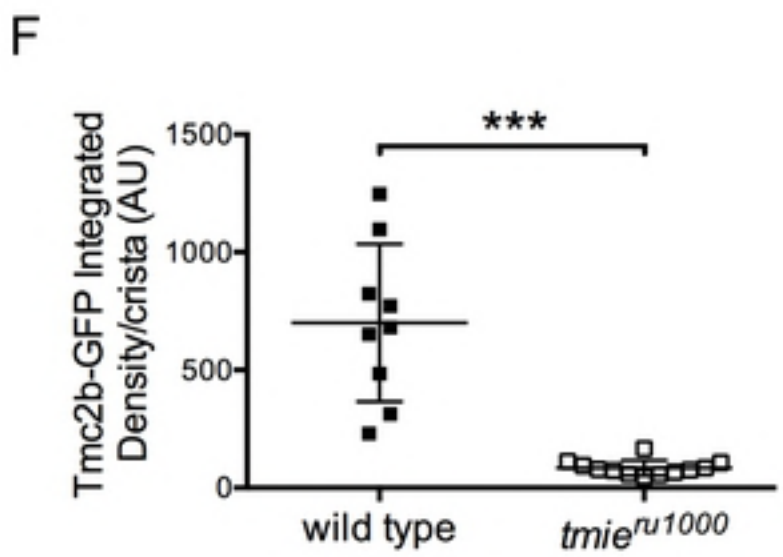
F
***
Tmc2b-GFP Integrated Density/crista (AU)
1500
1000
500
0
wild type
tmie ru1000

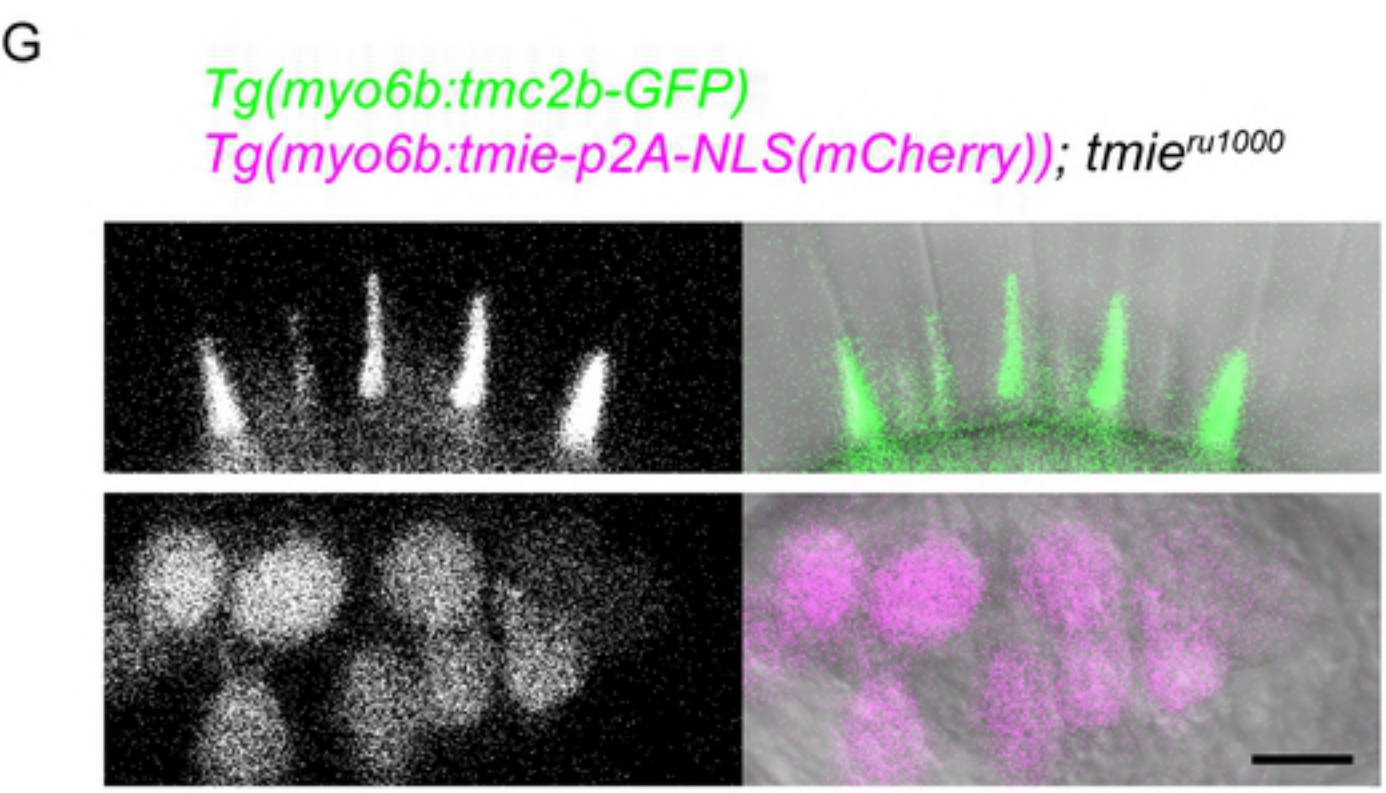
G
Tg(myo6b:tmc2b-GFP)
Tg(myo6b:tmie-p2A-NLS(mCherry)); tmie ru1000

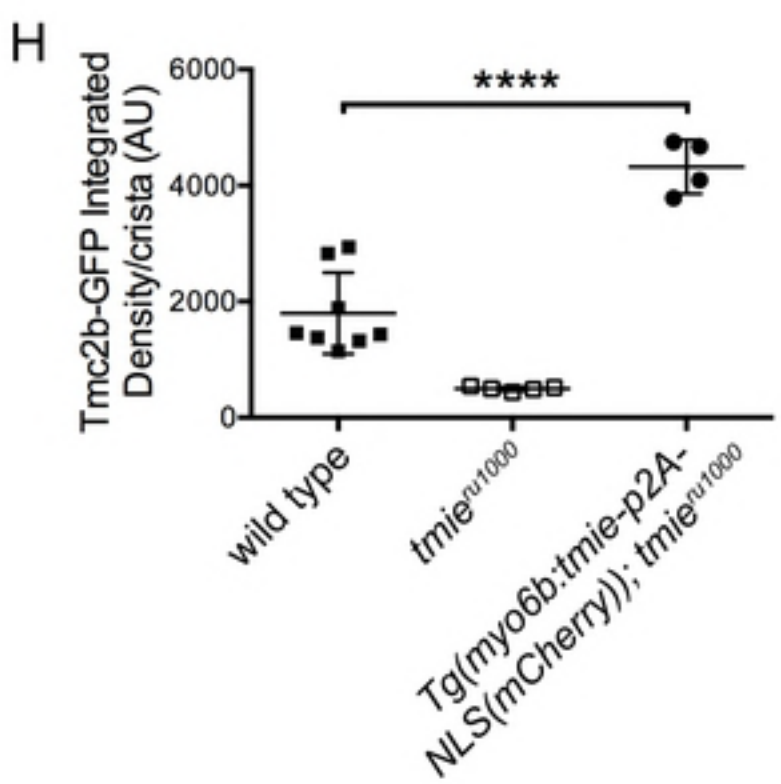
H
****
Tmc2b-GFP Integrated Density/crista (AU)
6000
4000
2000
0
wild type
tmie ru1000
Tg(myo6b:tmie-p2A-NLS(mCherry)); tmie ru1000

A

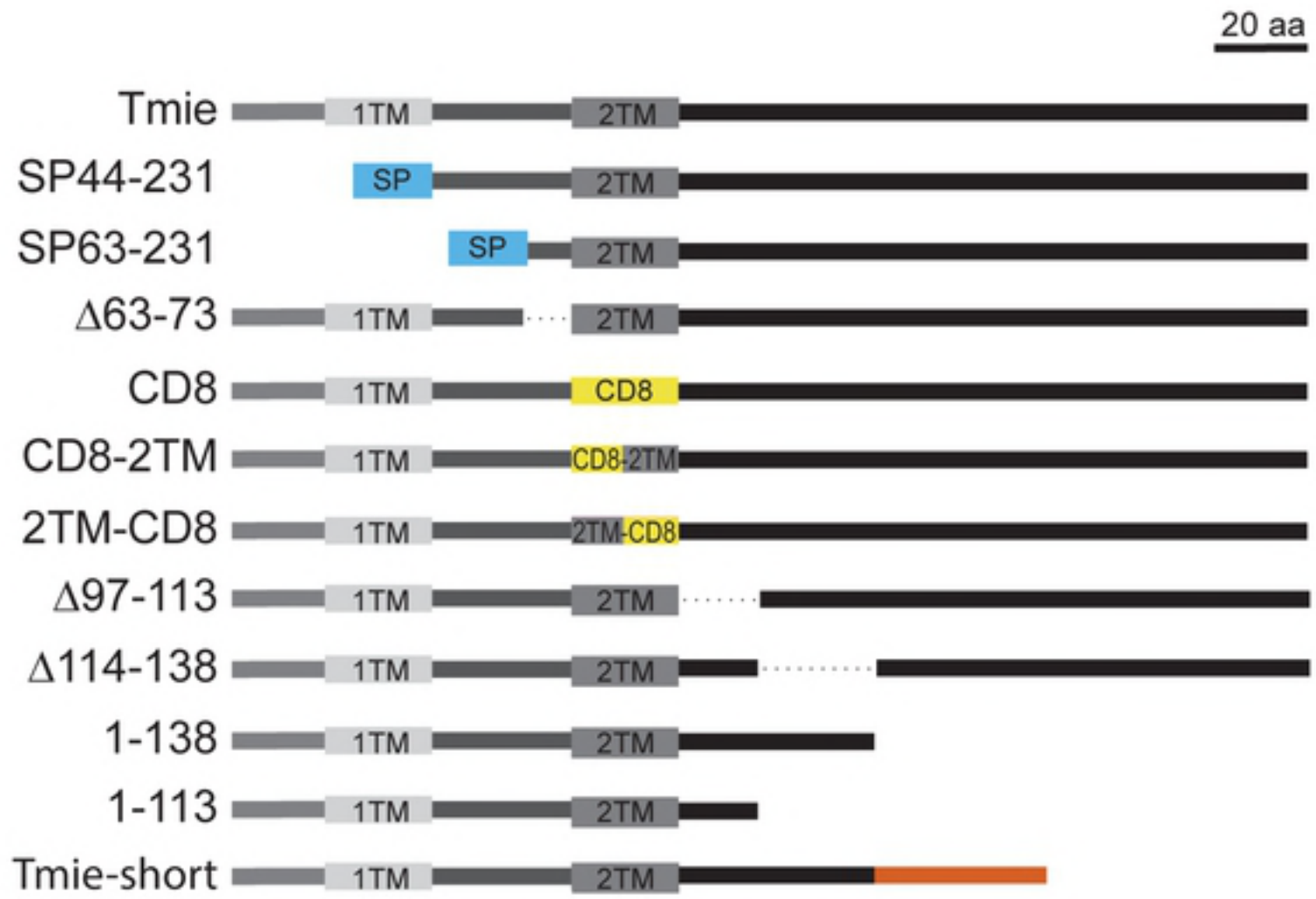
20 aa
Tmie
SP44-231
SP63-231
Δ63-73
CD8
CD8-2TM
2TM-CD8
Δ97-113
Δ114-138
1-138
1-113
Tmie-short
1TM
2TM
SP
CD8

B

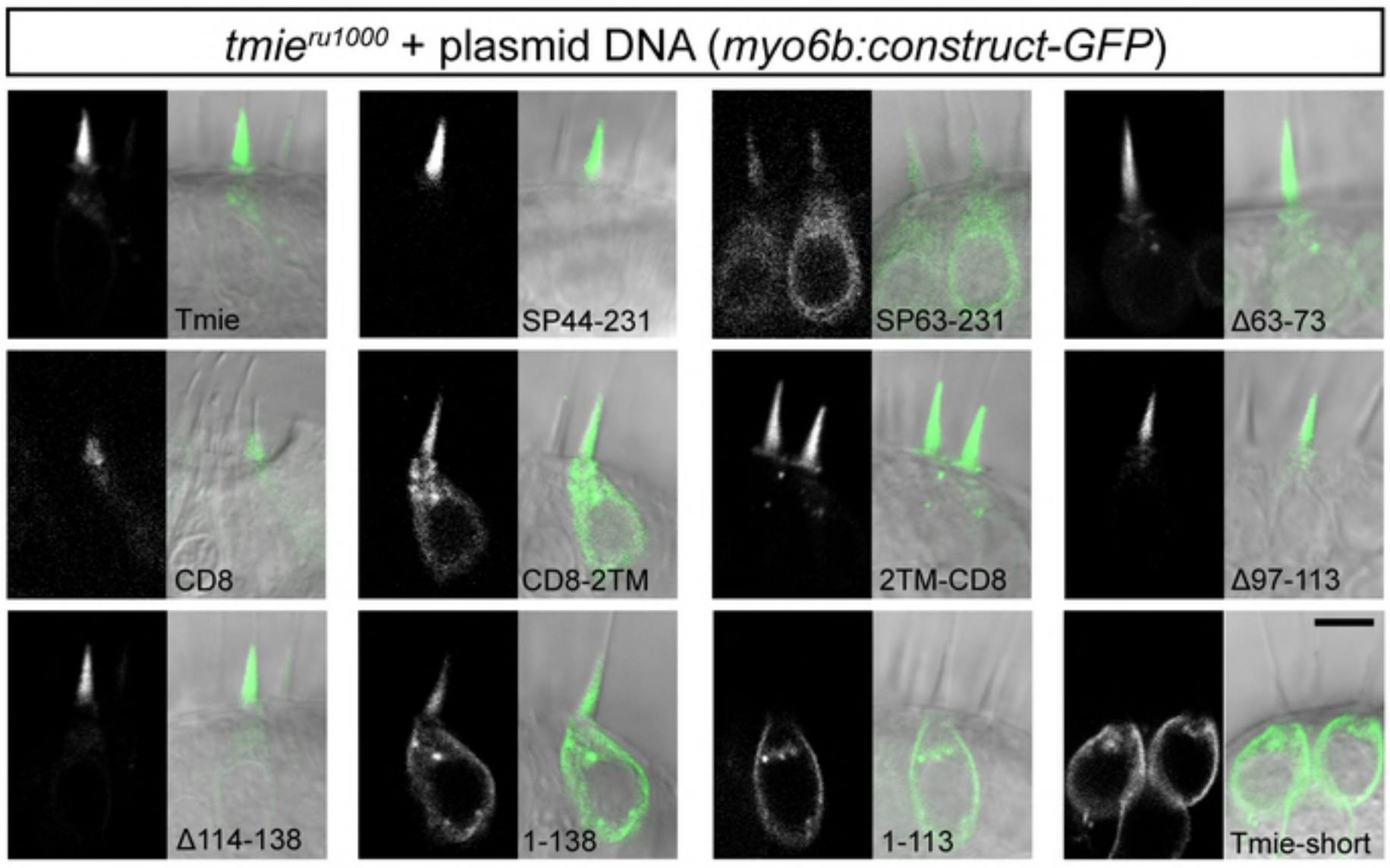
tmie ru1000 + plasmid DNA (myo6b:construct-GFP)
Tmie
SP44-231
SP63-231
Δ63-73
CD8
CD8-2TM
2TM-CD8
Δ97-113
Δ114-138
1-138
1-113
Tmie-short

C

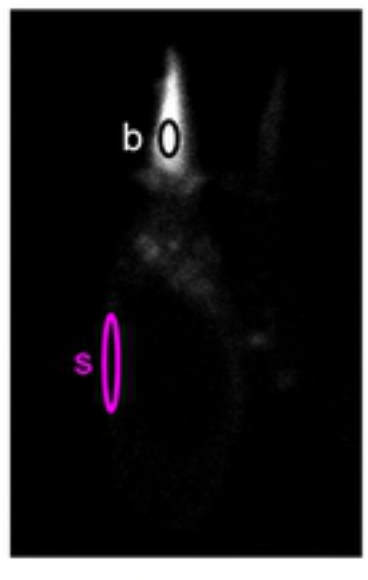
b
s

D

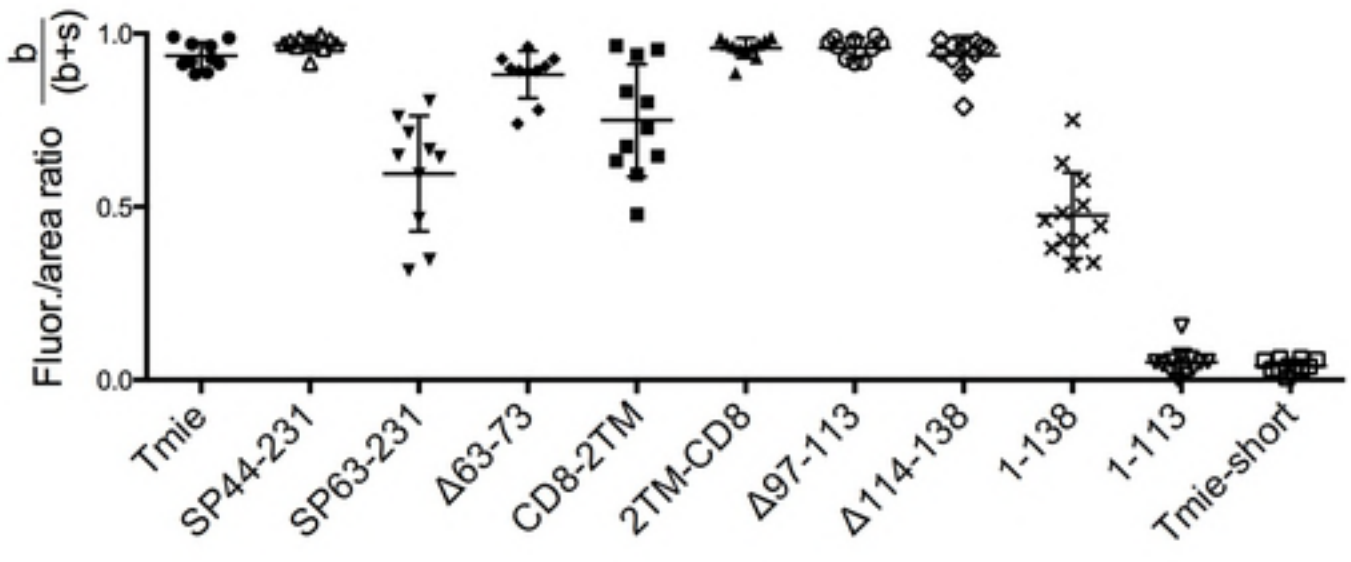
Fluor./area ratio
b / (b+s)
1.0
0.5
0.0
Tmie
SP44-231
SP63-231
Δ63-73
CD8-2TM
2TM-CD8
Δ97-113
Δ114-138
1-138
1-113
Tmie-short

A

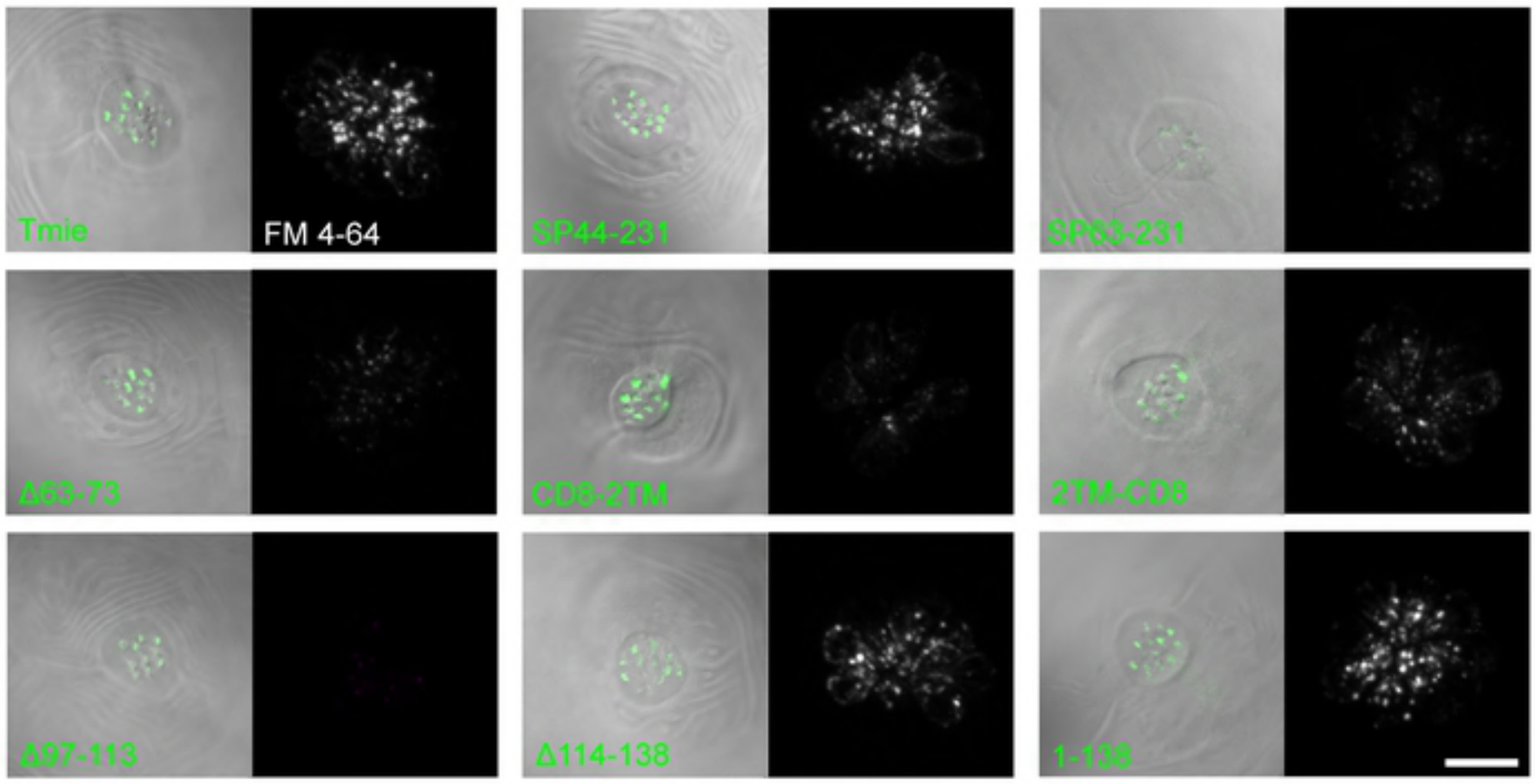
Tg(myo6b:construct-GFP); tmie ru1000
Tmie
FM 4-64
SP44-231
SP63-231
Δ63-73
CD8-2TM
2TM-CD8
Δ97-113
Δ114-138
1-138

B

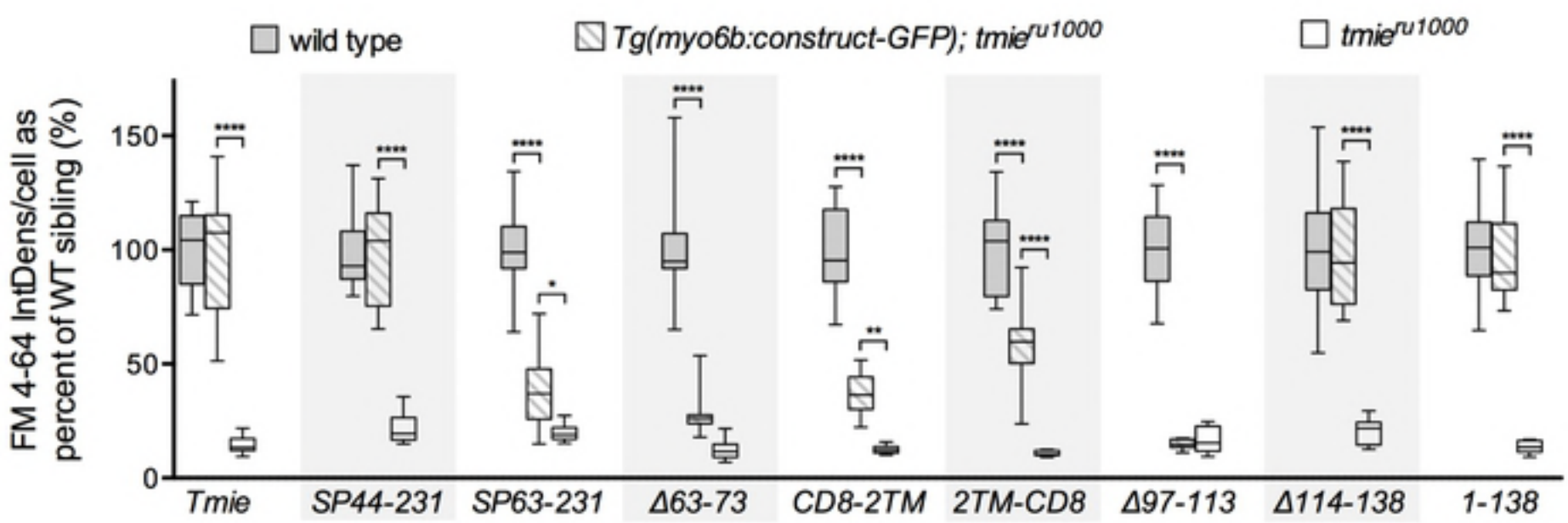
wild type
Tg(myo6b:construct-GFP); tmie ru1000
tmie ru1000
FM 4-64 IntDens/cell as percent of WT sibling (%)
150
100
50
0
Tmie
SP44-231
SP63-231
Δ63-73
CD8-2TM
2TM-CD8
Δ97-113
Δ114-138
1-138

C

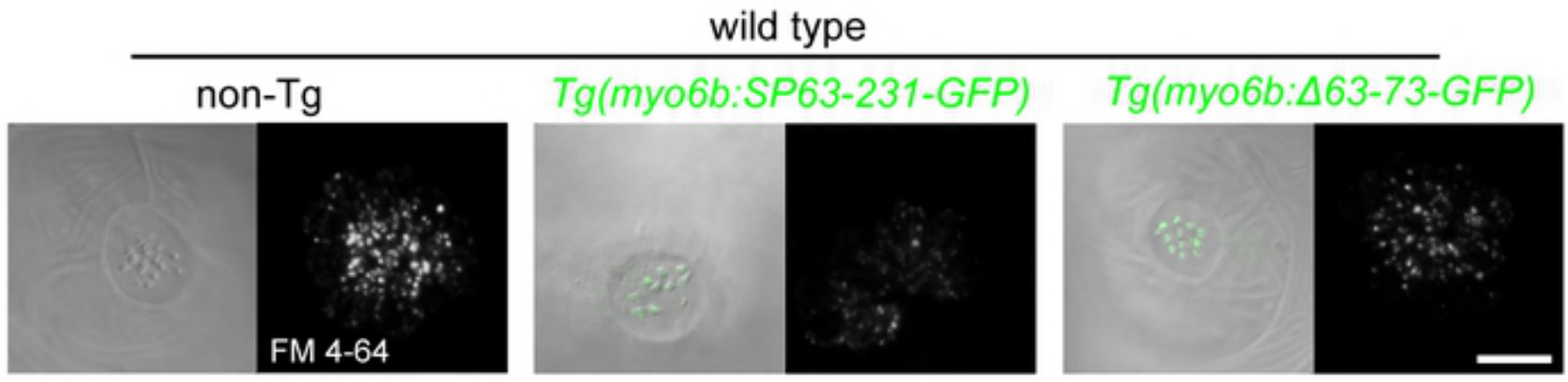
wild type
non-Tg
Tg(myo6b:SP63-231-GFP)
Tg(myo6b:Δ63-73-GFP)
FM 4-64

D

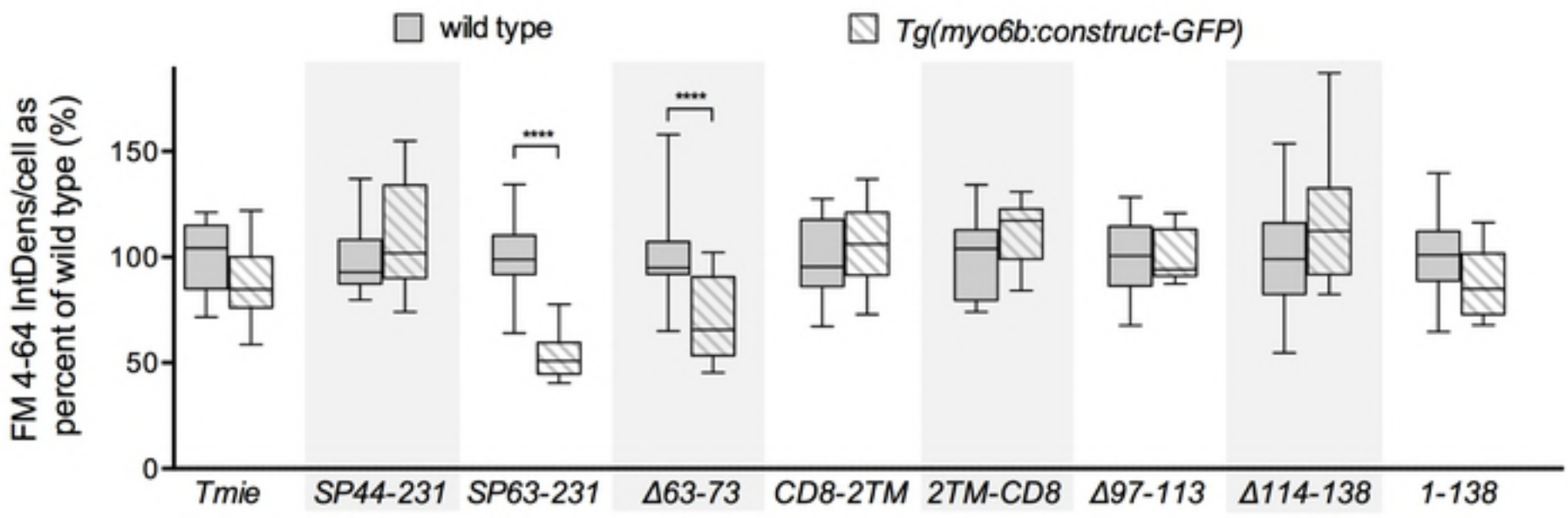
wild type
Tg(myo6b:construct-GFP)
FM 4-64 IntDens/cell as percent of wild type (%)
150
100
50
0
Tmie
SP44-231
SP63-231
Δ63-73
CD8-2TM
2TM-CD8
Δ97-113
Δ114-138
1-138

wild type
Tg(myo6b:construct-GFP)
tmie ru1000
Tg(myo6b:construct-GFP); tmie ru1000

A

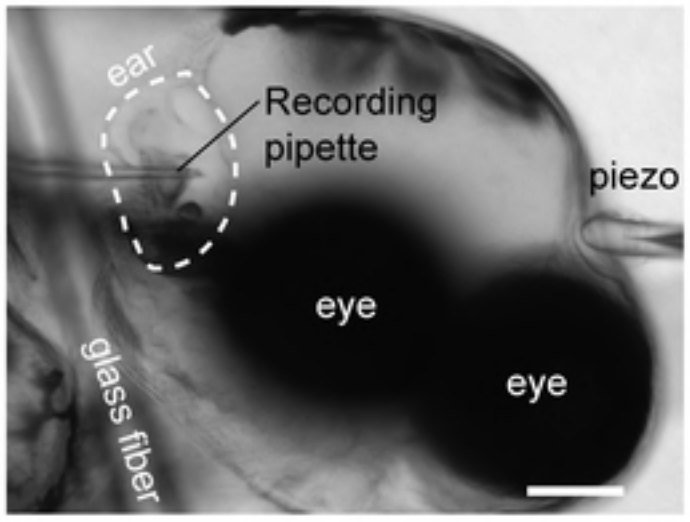

B

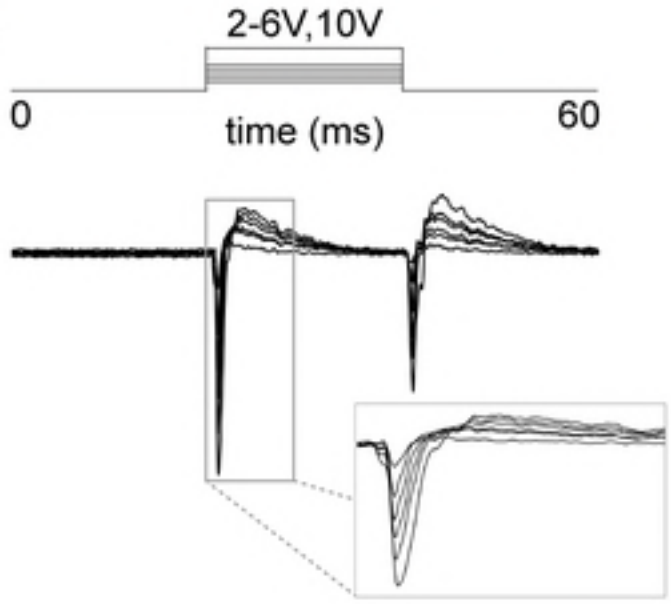

C

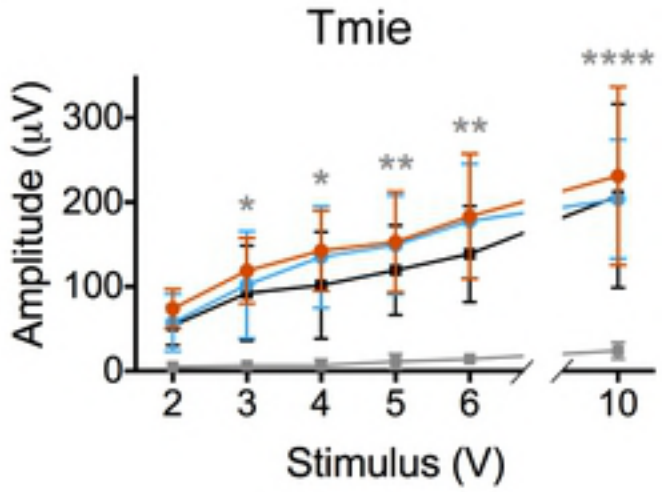

D

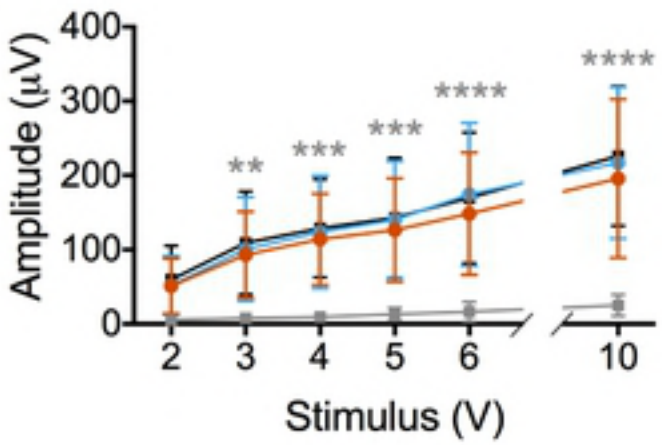

E

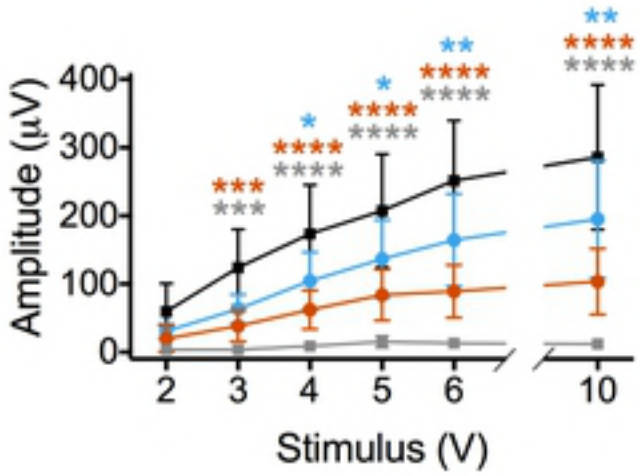

F

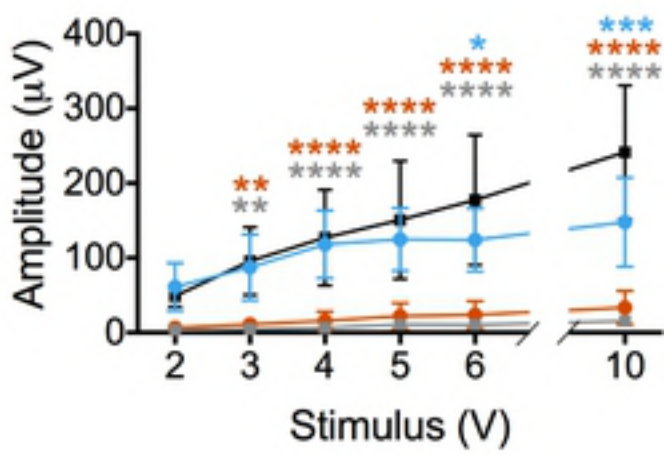

G

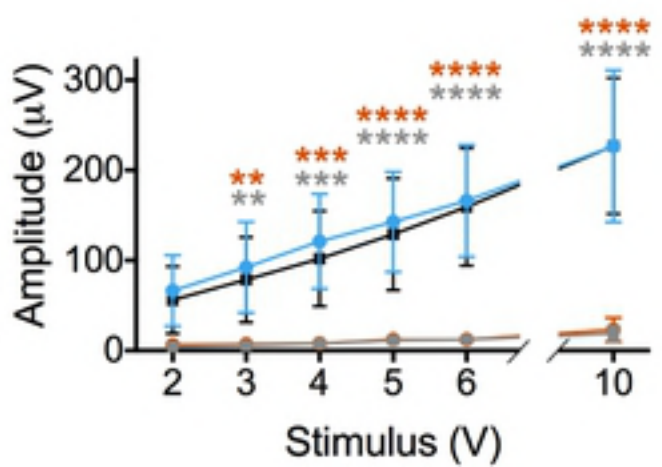

H

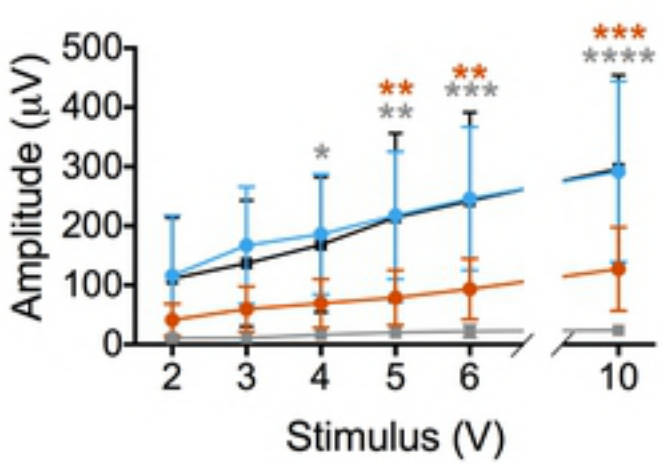

I

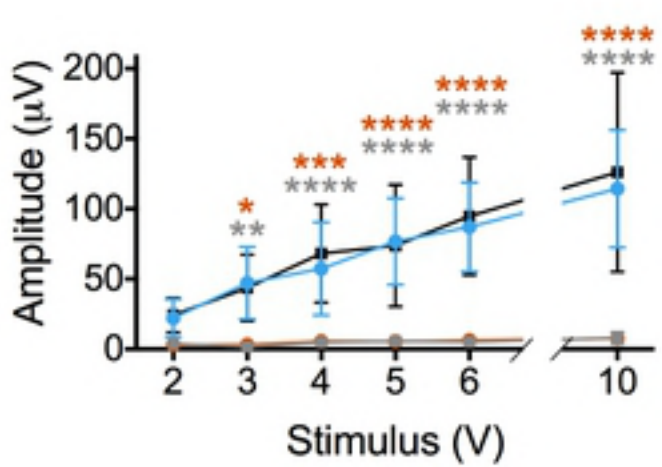

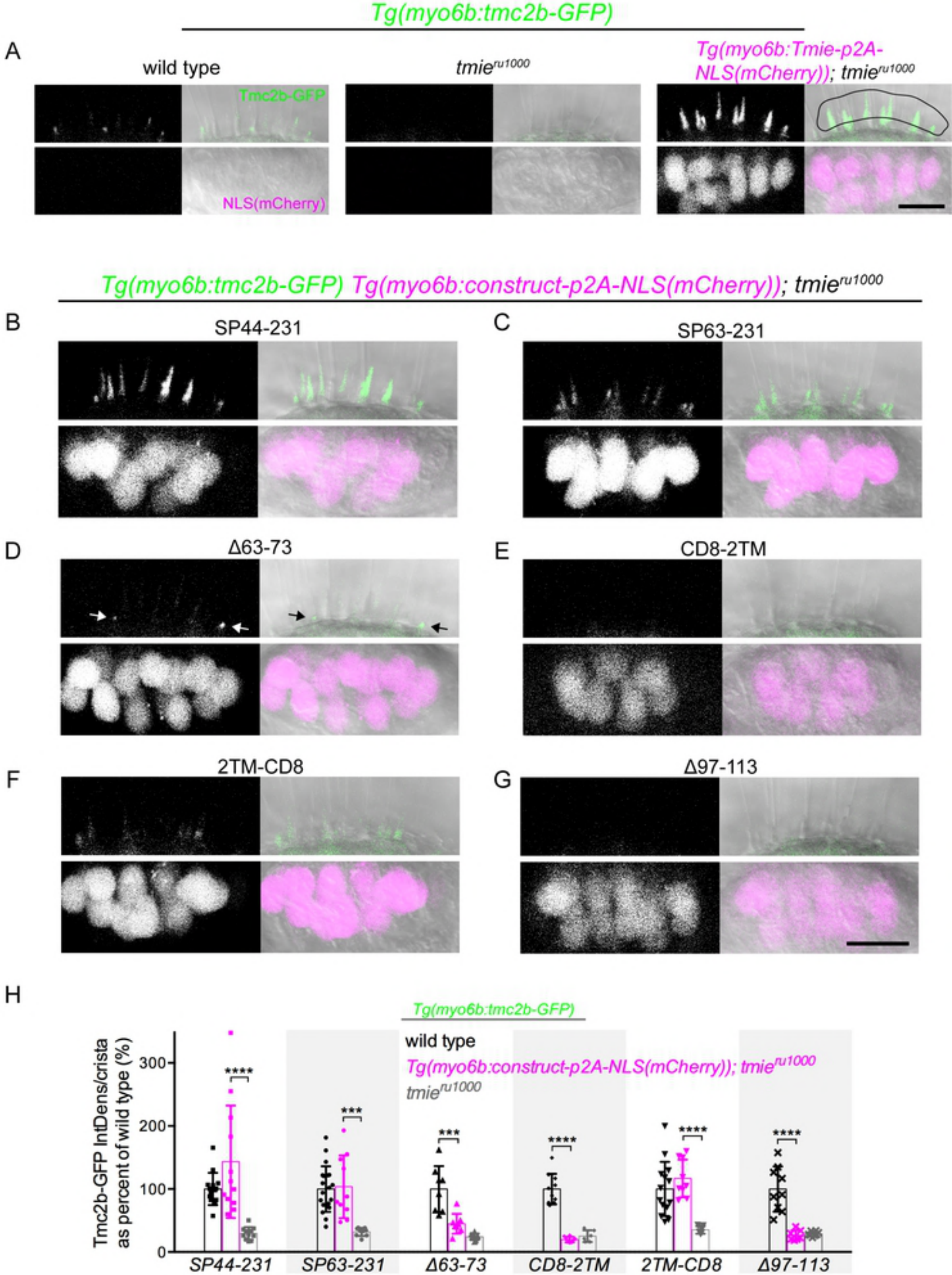
Tg(myo6b:tmc2b-GFP)
A
wild type
tmie ru1000
Tg(myo6b:Tmie-p2A-NLS(mCherry)); tmie ru1000
Tmc2b-GFP
NLS(mCherry)
Tg(myo6b:tmc2b-GFP) Tg(myo6b:construct-p2A-NLS(mCherry)); tmie ru1000
B
SP44-231
C
SP63-231
D
Δ63-73
E
CD8-2TM
F
2TM-CD8
G
Δ97-113
H
Tg(myo6b:tmc2b-GFP)
wild type
Tg(myo6b:construct-p2A-NLS(mCherry)); tmie ru1000
tmie ru1000
Tmc2b-GFP IntDens/crista as percent of wild type (%)
300
200
100
0
****
***
SP44-231
SP63-231
Δ63-73
CD8-2TM
2TM-CD8
Δ97-113

A

20 aa

	self-trafficking to bundle	self-stability in bundle	FM dye assay	microphonics assay	dominant negative effect	trafficking of Tmc to bundle	stability of Tmc in bundle
Tmie	+	+	+	+	-	++	+
SP44-231	+	+	+	+	-	+	+
SP63-231	+/-	+	+/-	+/-	+	+	+
Δ63-73	+	+	-	-	+	+	-
CD8	+	-					
CD8-2TM	+/-	+	+/-	-	-	-	
2TM-CD8	+	+	+/-	+/-	-	+	+
Δ97-113	+	+	-	-	-	-	
Δ114-138	+	+	+		-		
1-138	+/-	+	+		-		
1-113	-						
Tmie-short	-						

B

Tmie

Non-essential

extracellular

cytoplasmic

Yellow glow: Dominant negative effect when deleted

Effect on Tmie (self)

Blue outline: Self-targeting to the bundle

G Orange lettering: Self-stabilizing in the bundle

* Asterisk: Truncation ablates self-targeting to the bundle

Effect on Tmcs

Yellow fill: Targeting of Tmcs to the bundle

Orange fill: Stabilization of Tmc expression in the bundle